Interplay between disorder and electron interactions in a $d=3$ site-disordered Anderson-Hubbard model: A numerical mean-field study

Michael A. Tusch and David E. Logan
University of Oxford, Physical Chemistry Laboratory, South Parks Road, Oxford OX1 3QZ, United Kingdom
(Received 21 April 1993; revised manuscript received 28 June 1993)

We consider a numerical mean-field study, at the unrestricted Hartree-Fock level, of a Gaussian site-disordered Anderson-Hubbard model on a simple cubic lattice. The phase diagram at half filling is obtained, including magnetic and metallic-insulating phases, and all relevant phase boundaries are found to occur in a relatively weak-coupling regime. Variation with filling fraction y is also considered, with particular reference to the y-differential disorder-induced enhancement of electron interactions that lead to site-differential local-moment formation. The inhomogeneous distribution of local charges and magnetic moments over the sites is found to influence strongly the distribution and character of pseudoparticle states. This enables a simple microscopic rationalization of the metal-insulator transition and its phase boundaries in terms of an interplay between disorder and electron interactions, giving in addition a natural explanation for the two-fluid-like coexistence of delocalized charge-carrying states and strong-local-moment sites.

I. INTRODUCTION

Understanding the combined effects of disorder and electron interactions is a central issue in condensed-matter physics. The problem has thus attracted great interest (see, e.g., Refs. 1–22) by a wide variety of methods, although much remains to be learned—even qualitatively—about the interplay between disorder and interaction effects.

We describe here a detailed numerical study, at a mean-field level, of perhaps the simplest model with which to study the simultaneous occurrence of disorder and interactions: a one-band disordered Anderson-Hubbard model (AHM) with uncorrelated site disorder, in $d=3$ for a simple cubic lattice, and with nearest-neighbor hopping matrix elements $T_{ij}=-T$.[13–17] The model Hamiltonian is

$$H=\sum_{i,\sigma}\epsilon_i n_{i\sigma}-T\sum_{\langle ij\rangle,\sigma}c_{i\sigma}^{\dagger}c_{j\sigma}+U\sum_i n_{i+}n_{i-}\ , \tag{1.1}$$

with $n_{i\sigma}=c_{i\sigma}^{\dagger}c_{i\sigma}$, $\sigma=\pm$ denoting the spins, and the $\langle ij\rangle$ sum over nearest-neighbor sites. On-site electron interactions are embodied in the repulsive Hubbard U, and the site energies $\{\epsilon_i\}$ are here regarded as independent random variables drawn from a Gaussian distribution $g(\epsilon)$ of variance Δ^2. The model is thus characterized by three parameters: $\tilde{U}=U/B$, a scaled measure of the interaction strength, with $B=12$ T the unperturbed ($U=0=\Delta$) simple cubic bandwidth; $\tilde{\Delta}=\Delta/B$, a scaled measure of the site disorder; and the electron filling fraction $y=N_e/N$, the ratio of the number of electrons (N_e) to sites (N).

Granted a finite-size numerical study, no approximations are made here in treating the site disorder. Interactions are treated at the unrestricted Hartree-Fock (UHF) level, which, for any disorder realization, is a mean-field approximation whose study we believe is justified for several reasons: (i) It is central in describing the instabilities to local moment formation, a feature of particular importance in disordered systems where local moment formation occurs on an inhomogeneous scale.[18,21] With disorder present, a rich range of physical behavior is captured at a UHF level, as is evident from recent work on both spatially disordered[18,22] and site-disordered[20,21] AHM's. (ii) As discussed below, UHF also provides an adequate description of the limits of the model and permits ready examination of the system in a wide region of the $(\tilde{\Delta},\tilde{U})$ phase plane between these limits. The resultant metallic-insulating and magnetic phase boundaries at half filling are in fact found here to occur in a relatively weak-coupling $\tilde{U}$ regime where UHF for the ground state is likely to be quite reasonable. (iii) UHF is amenable to systematic improvement, forming a natural starting point for inclusion of many-body correlations. In the strong-coupling limit of the pure $d=2$ Hubbard model, for example, a random-phase approximation (RPA) about the half-filled UHF ground state yields the exact linear spin-wave spectrum of the spin-$\frac{1}{2}$ Heisenberg model (see, e.g., Ref. 23), and a one-loop correction to the sublattice magnetization[23(b)] gives excellent agreement with $d=2$ Monte Carlo studies. With disorder present, a knowledge of the inhomogeneous mean-field ground states is thus a necessary prerequisite in this regard.

For these reasons, and also for its physical clarity, we believe a mean-field approach such as UHF to be at least a natural starting point for the model system with both disorder and interactions present. With it, we attempt here to gain a broad microscopic picture of the interplay between disorder and electron interactions. In Secs. II–IV we focus on half-filling, $y=1$, with particular reference to the $(\tilde{\Delta},\tilde{U})$ phase diagram. In Sec. II we describe briefly the UHF approximation employed and the measures used to determine the character of the phases. Section III gives our assessment of the magnetic phase diagram, and the antiferromagnetic, spin glasslike and

paramagnetic phases. In Sec. IV we consider metallic-insulating behavior and the metal-insulator transitions (MIT). The dominant type of MIT in the $(\tilde{\Delta},\tilde{U})$ plane for $y=1$ is the M-(gapless)IT occurring when pseudoparticle states at the Fermi level E_F become localized; although we also find a direct metal to Hubbard insulator transition confined to a very narrow region of the phase plane at small but nonzero disorder $\tilde{\Delta}$.

In Secs. V and VI we extend the work to filling fractions $y<1$, considering the evolution of the system with y up to half filling for representative points in the $(\tilde{\Delta},\tilde{U})$ plane. The motivation for this is described in Sec. V. Since states towards the lower edge of the $\tilde{U}=0$ noninteracting spectrum are increasingly strongly localized, the disorder-induced enhancement of interactions in leading to local moment formation may be differential in the filling fraction y. In particular, and in contrast to nondisordered systems, it has been argued[21] that a "quasiatomic" regime of strong local moments and mainly singly occupied nonoverlapping pseudoparticle states must consequently result for low y, regardless of whether the interaction strength $\tilde{U}$ is large enough to ensure the existence of moments at half-filling. This is considered in Sec. VI. The existence and characteristics of the quasiatomic regime are described in Sec. VI A; the evolution of the system with y beyond the quasiatomic y domain and up to half-filling is considered in Sec. VI B; and the variation of results with $\tilde{U}$ and $\tilde{\Delta}$ is discussed in Sec. VI C. A brief summary is given in Sec. VII.

Throughout the paper we attempt to give a microscopic rationale for observed behavior, central to which is the inhomogeneous distribution of local magnetic moments (and charges) over the sites. These, for example, will be shown to determine the *sites* which typically give the dominant contribution to pseudoparticle *states* at E_F (thus providing evidence for a recently suggested[21] parallel to the single-impurity Anderson model[24]), and may in turn be related to the localization characteristics of the Fermi-level pseudoparticle states, and hence to the MIT.

Before proceeding we comment on the limits of the model, the simplest of which is the atomic limit $B=12$ $T=0$. The Gaussian site energy distribution $g(\epsilon)$ is shown in Fig. 1(A), and from particle-hole symmetry (which is preserved for $B\neq 0$) the Fermi level $E_F(y)=U-E_F(2-y)$, such that at half filling $E_F(1)=\frac{1}{2}U$. From stability of the atomic limit ground state to particle-hole excitations, sites in an ϵ interval of width U below $E_F(y)$ are the singly occupied local moment sites, with a charge and local moment magnitude of unity. All other sites are nonmagnetic, those with $\epsilon<E_F(y)-U$ being doubly occupied by electrons and those with $\epsilon>E_F(y)$ being empty, and at half filling in particular the fraction of moment carrying sites clearly increases with U/Δ. We also note that, regardless of the interaction strength U, and for any $\Delta>0$, there is no true Hubbard gap in the atomic limit single-particle spectrum $D(E)$ for any y. These features are correctly preserved at a UHF level.

The nontrivial limits of the model are the noninteracting ($\tilde{U}=0$) but disordered Anderson limit, where Eq. (1.1) reduces to a site-disordered tight-binding model, and

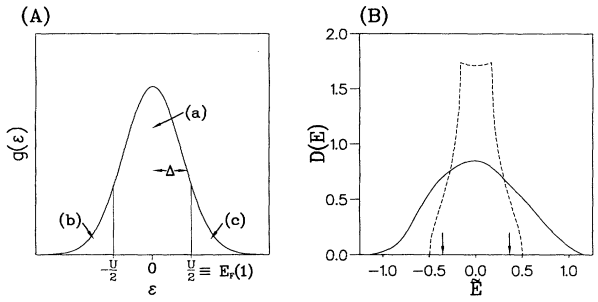

FIG. 1. (A) The Gaussian site energy distribution $g(\epsilon)$, with atomic limit site occupation illustrated for half filling: singly occupied local moment sites [region (a)], doubly occupied sites (b), and unoccupied sites (c). (B) Disorder-averaged $D(E)$ vs $\tilde{E}=E/B$ in the noninteracting limit for $\tilde{\Delta}=\frac{5}{12}$ and $N=10^3$ sites; mobility edges in $D(E)$ (Ref. 26) are indicated by arrows. The unperturbed simple cubic spectrum (dashed line) is shown for comparison.

the nondisordered ($\tilde{\Delta}=0$) pure Hubbard model. For $\tilde{U}=0$, Anderson localization of states at $E_F(y)$ leads to a pure disorder-induced MIT at a critical value $\tilde{\Delta}_c(y)$ of the scaled disorder. With a Gaussian $g(\epsilon)$ it is known[25–27] that for $\tilde{\Delta}>\frac{1}{2}$ all states in the noninteracting spectrum are localized. At $\tilde{\Delta}=\frac{1}{2}$, $E=0$ band center states become delocalized, and for $\tilde{\Delta}<\frac{1}{2}$ both localized and extended states occur, separated by mobility edges at $\pm E_c$; mobility edge trajectories are considered in Refs. 25–27. Thus, at half filling $\tilde{\Delta}_c(1)=\frac{1}{2}$, while $\tilde{\Delta}_c(y)<\frac{1}{2}$ for $y<1$. Figure 1(B) shows the disorder-averaged single particle spectrum $D(E)$ for $\tilde{U}=0$ and $\tilde{\Delta}=\frac{5}{12}$, obtained numerically for $N=10^3$ sites; the unperturbed simple cubic spectrum is also shown, in terms of whose bandwidth B all energies are scaled. States at $\tilde{E}=0$ [$\equiv\tilde{E}_F(1)$] are extended at the chosen $\tilde{\Delta}$, and mobility edges (from Ref. 26) are shown.

At half filling, $y=1$, and for bipartite lattices such as the simple cubic, the ground state of the pure Hubbard model is believed generically to be a two-sublattice antiferromagnetic insulator for all $U>0$ (see, e.g., Refs. 28–30). In contrast to some many-body approaches, this feature is preserved at a UHF level, where the $y=1$ ground state is a uniform Néel antiferromagnet with a Hubbard gap in the single particle spectrum $D(E)$ for any nonzero U.[31] The effect arises from the Fermi surface nesting characteristic of the unperturbed simple cubic lattice, a feature we anticipate obviated by the presence of disorder, leading for suitably small but nonzero $\tilde{\Delta}$ to the possibility of a paramagnetic metal to antiferromagnetic metal to antiferromagnetic insulator sequence with increasing $\tilde{U}$, which is typical of the pure half-filled Hubbard model for nonbipartite cubic lattices (see, e.g., Ref. 32).

II. UHF

The most general form of UHF is the spin-rotationally invariant "Heisenberg-spin" form. In view, however, of

the expected dominance at half filling of $S_z^{\rm tot}=0$ Ising-like UHF ground states, we here consider explicitly "Ising-spin" UHF where the single-particle states are pure spin orbitals. The validity of this approach has been checked for a range of points in the $(\tilde{\Delta},\tilde{U})$ phase plane for $y=1$ by (a) investigation of the stability matrix,[33] which, if positive definite or semidefinite, shows the Ising-like solutions under test to be at least locally stable with respect to RPA-like collective particle-hole excitations; and (b) direct implementation of the Heisenberg-spin UHF. In all cases the Ising-like solutions we consider were found to be stable.

For any disorder realization the spin-separable Ising-spin UHF Hamiltonian is

$$H=\sum_{i,\sigma}\epsilon_{i\sigma}n_{i\sigma}-T\sum_{\langle ij\rangle,\sigma}c_{i\sigma}^{\dagger}c_{j\sigma}\equiv\sum_{\sigma}H_{\sigma}\ . \tag{2.1}$$

The effective σ-spin site energy $\epsilon_{i\sigma}$ $(\sigma=\pm)$ is given by

$$\epsilon_{i\sigma}=\epsilon_i+U\bar{n}_{i-\sigma}=\epsilon_i+\tfrac{1}{2}U[n_i-\sigma\mu_i]\ , \tag{2.2}$$

where $\{\bar{n}_{i\sigma}\}$ are the mean occupation numbers in the UHF ground state, and we have introduced the site local charge n_i and local magnetic moment μ_i $(=2\bar{s}_{iz})$ given by

$$n_i=\bar{n}_{i+}+\bar{n}_{i-}\ ,\quad \mu_i=\bar{n}_{i+}-\bar{n}_{i-}\ . \tag{2.3}$$

Pseudoparticle states are found from $H_{\sigma}|\Psi_{\alpha\sigma}\rangle=E_{\alpha\sigma}|\Psi_{\alpha\sigma}\rangle$ with $|\Psi_{\alpha\sigma}\rangle=\sum_i a_{i\alpha\sigma}|\phi_{i\sigma}\rangle$ expanded in the site basis, together with the self-consistency equations $\bar{n}_{i\sigma}=\sum_{\alpha<E_F}|a_{i\alpha\sigma}|^2$ for the $\{\bar{n}_{i\sigma}\}$. Since $H_{\sigma}\equiv H_{\sigma}(\{\bar{n}_{i-\sigma}\})$, an iterative self-consistency procedure is implied, and the equations are solved numerically by Lanczos diagonalization[34] at each iteration step. This allows us to study quite large systems (up to $N=10^3$) despite the need to average over many disorder realizations of the bare site energies $\{\epsilon_i\}$ for each $(\tilde{\Delta},\tilde{U})$ point. The principal limitation is that Lanczos degeneracies preclude direct examination of the $\tilde{\Delta}\rightarrow 0$ limit. We find, however, that values of $\tilde{\Delta}$ as low as 0.025 can be employed without difficulty, and the $\tilde{\Delta}=0$ pure Hubbard limit for $y=1$ is in any event soluble analytically at the UHF level (see, e.g., Ref. 31).

To map out the phases at half-filling we obtained self-consistent solutions for several hundred points in the $(\tilde{\Delta},\tilde{U})$ plane, and for each point a sufficient number of disorder realizations was considered to give adequate statistics (up to 20 near phase boundaries). In general, many stable UHF solutions may coexist for a given disorder realization at a given $(\tilde{\Delta},\tilde{U})$ point. By repeating the calculations for several different initial or input states—including uniform Néel antiferromagnets (AF's), disordered AF configurations with input $\{n_i,|\mu_i|\}$ derived from the atomic limit $B=12T=0$, paramagnetic states (via restricted HF), and states with random initial charge-spin distributions—we explore a good proportion of the possible final or converged solutions. Since UHF is variational, our criterion for the nature of the ground state is energetic, as discussed further in Sec. III.

For a given disorder realization at any $(\tilde{\Delta},\tilde{U})$ point, the distribution of self-consistent local charges and magnetic moment magnitudes over the sites may be characterized by the mean charge and local moment magnitude per site of energy ϵ, viz.

$$n(\epsilon)=N_{\epsilon}^{-1}\sum_{i:\epsilon_i=\epsilon}n_i\ ,\quad |\mu(\epsilon)|=N_{\epsilon}^{-1}\sum_{i:\epsilon_i=\epsilon}|\mu_i|\ , \tag{2.4}$$

where N_{ϵ} is the number of sites with bare site energy ϵ, such that $N_{\epsilon}/N=g(\epsilon)d\epsilon$. In the $B=12T=0$ atomic limit described in Sec. I, for example, n_i (and $|\mu_i|$) has the same value for all sites with a given $\epsilon_i=\epsilon$, whence $|\mu(\epsilon)|=\min[n(\epsilon),2-n(\epsilon)]$ with $n(\epsilon)=0$, 1, or 2 according to site occupancy; see Fig. 1(a).

The bulk magnetic character of converged UHF solutions is determined by magnetic ordering (or otherwise) of the local moments, reflected in the relative phases of the $\{\mu_i\}$. To characterize this we follow Dasgupta and Halley[20] and examine the Fourier transform of the z component of the spin density,

$$S_z(\mathbf{k})=\frac{1}{N}\sum_i\mu_i\exp(i\mathbf{k}\cdot\mathbf{R}_i)\ . \tag{2.5}$$

A disordered AF phase, for example, produces an $|S_z(\mathbf{k})|$ sharply peaked at $\mathbf{k}a/\pi=(1,1,1)$ (with a the lattice spacing) on the order of the mean local moment magnitude per site; a spin-glass (SG) phase gives numerous small peaks in $|S_z(\mathbf{k})|$ with none dominant; and a paramagnetic (P) state has $\mu_i=0$ for all sites. These are considered in Sec. III.

For any disorder realization, relevant densities of single-particle excitations (DOS), or pseudoparticle spectra, also follow directly. The total (normalized) DOS is $D(E)=\frac{1}{2}\sum_{\sigma}D_{\sigma}(E)$, where the total σ-spin DOS is given by

$$D_{\sigma}(E)=N^{-1}\sum_{\alpha}\delta(E-E_{\alpha\sigma})=N^{-1}\sum_i D_{i\sigma}(E)\ , \tag{2.6a}$$

with

$$D_{i\sigma}(E)=\sum_{\alpha}|a_{i\alpha\sigma}|^2\delta(E-E_{\alpha\sigma}) \tag{2.6b}$$

the local σ-spin DOS for site i; with $S_z^{\rm tot}\equiv S_z(\mathbf{k}=\mathbf{0})=0$, $D_{\sigma}(E)=D_{-\sigma}(E)$ holds on the average (or, for a given disorder realization, in the $N\rightarrow\infty$ limit). It is also helpful to introduce[21] an ϵ-resolved local DOS, $D(\epsilon;E)=\frac{1}{2}\sum_{\sigma}D_{\sigma}(\epsilon;E)$, where

$$D_{\sigma}(\epsilon;E)=N_{\epsilon}^{-1}\sum_{i:\epsilon_i=\epsilon}D_{i\sigma}(E) \tag{2.7}$$

is the mean local DOS per site of energy ϵ, and in terms of which

$$D(E)=\int_{-\infty}^{\infty}D(\epsilon;E)g(\epsilon)d\epsilon\ . \tag{2.8}$$

The total DOS is thus a composite of the local spectra $D(\epsilon;E)$ which, if sites of energy ϵ possess local moments, will be shown in Secs. IV and VI to consist of overlapping but resolved lower and upper local Hubbard subbands.

The M-(gapless)IT occurs when pseudoparticle states at the Fermi level $E_F(y)=[U-E_F(2-y)]$ become localized. To assess directly the localized or extended charac-

ter of pseudoparticle states of energy E (and at E_F in particular) we consider the mean inverse participation ratio (IPR): $\bar{L}(E)$, where an overbar here denotes a disorder average for pseudoparticle states of both spins within a narrow range $E\pm 0.025B$. For a single σ-spin pseudoparticle state of energy $E_{\alpha\sigma}=E$, $L(E)=\sum_i |a_{i\alpha\sigma}|^4$ and $\sim 1/m$ for a state uniformly spread over m sites. In the thermodynamic limit $L(E)$ is thus zero for a delocalized state and non-zero for a localized state with magnitude roughly the inverse of the number of sites participating in the state. For a finite system, $L(E)>0$ necessarily, but the location of mobility edges may be estimated satisfactorily from a threshold mean IPR, $\bar{L}_c$, appropriate to a particular system size, such that for $\bar{L}(E)>\bar{L}_c$ [$\bar{L}(E)<\bar{L}_c$] states of energy E may be deemed localized [extended]. In the noninteracting limit, this threshold has been addressed via a finite-size scaling analysis by Chang, Bauer, and Skinner,[27] who find $\bar{L}_c$ to scale with system size as

$$\bar{L}_c \simeq 1.14/N^{0.48} . \tag{2.9}$$

To estimate the M-(gapless)I phase boundary in the present case, Eq. (2.9) will be used for $\bar{L}_c$. For $N=512$ sites, the resultant $\bar{L}_c \simeq 0.06$ indeed reproduces correctly $\tilde{\Delta}_c(1)=\frac{1}{2}$ for $\tilde{U}=0$ (see Fig. 2).[25-27] Although the effect of U on the N scaling of $\bar{L}_c$ is not known (and a computational determination of it would be prohibitively expensive), the location and features of the MIT phase boundary are not sensitive to the chosen $\bar{L}_c$, as discussed further in Sec. IV [and as is evident from the $y=1$ Fermi level IPR profile in the $(\tilde{\Delta},\tilde{U})$ plane, Fig. 5].

While the IPR is an important diagnostic in assessing the character of pseudoparticle states, it gives little direct physical insight into why the states are localized or extended. Localization of pseudoparticle states stems ultimately from disorder inherent in the distribution of effective σ-spin site energies $\{\epsilon_{i\sigma}\}$ which enter the UHF Hamiltonian H_σ of Eq. (2.1); and since $\epsilon_{i\sigma}=\epsilon_i+\frac{1}{2}U[n_i-\sigma\mu_i]$, this arises both from explicit disorder in the bare $\{\epsilon_i\}$ [embodied in $g(\epsilon)$] and also from the charge-spin disorder reflected in the distribution of $\{n_i,\mu_i\}$. In order to determine the extent to which sites with different bare site energies ϵ contribute to pseudoparticle states of a given energy E—and thus to relate the nature of pseudoparticle *states*, at E_F in particular, to the self-consistent distribution of local magnetic moments over the *sites*—we consider the Fermi-level charge density $H(\epsilon;E_F)=\frac{1}{2}\sum_\sigma H_\sigma(\epsilon;E_F)$.[21] $H_\sigma(\epsilon;E)$ is the quantum probability density that electrons in σ-spin pseudoparticle states of given energy E will be found on sites with bare site energy ϵ and is given by

$$H_\sigma(\epsilon;E)=\frac{\sum_\alpha p(\epsilon;E_{\alpha\sigma})\delta(E_{\alpha\sigma}-E)}{\sum_\alpha \delta(E_{\alpha\sigma}-E)} , \tag{2.10}$$

where $p(\epsilon;E_{\alpha\sigma})=\sum_i |a_{i\alpha\sigma}|^2\delta(\epsilon_i-\epsilon)$ is the corresponding probability density for a single σ-spin state of energy $E_{\alpha\sigma}$. By definition $\int d\epsilon\, H_\sigma(\epsilon;E)=1$, and with $S_z^{\rm tot}=0$, $H_\sigma=H_{-\sigma}$ on the average (cf. the comments above regarding $D_\sigma=D_{-\sigma}$). Further, it is evident that $H_\sigma(\epsilon;E)$ is related to the pseudoparticle spectra defined above by

$$H_\sigma(\epsilon;E)=g(\epsilon)D_\sigma(\epsilon;E)/D_\sigma(E) . \tag{2.11}$$

Although $H(\epsilon;E_F)$ [or $H_\sigma(\epsilon;E_F)$] does not give direct information on localization it enables us, when combined with the IPR, to rationalize the localization characteristics of Fermi-level pseudoparticle states—and hence the M-(gapless)IT—in terms of site-differential local moment stability [reflected in $|\mu(\epsilon)|$]. Further, introduction in particular of the ϵ-resolved quantities enable contact with a recent statistical mean-field approach[21] to a site-disordered AHM (formulated at a coherent potential approximation level within a UHF framework), the results of which will be shown to be in good agreement with the present study.

III. $y=1$ MAGNETIC PHASES

Our assessment of the $y=1$ magnetic phases for $\tilde{U}<0.8$ and $0.05<\tilde{\Delta}<0.8$ is shown in Fig. 2. Representative examples of $|S_z(\mathbf{k})|$ are shown in Fig. 3 for (a) $(\tilde{\Delta},\tilde{U})=(\frac{5}{12},1)$ and (b) $(\tilde{\Delta},\tilde{U})=(\frac{5}{12},\frac{1}{2})$, where the system is a relatively clean antiferromagnet, and (c) $(\tilde{\Delta},\tilde{U})=(\frac{5}{12},0.15)$ as an example of a spin-glass-like phase.

For any disorder realization at a given $(\tilde{\Delta},\tilde{U})$ point, different initial or startup states give final or converged UHF solutions very close in energy, typically within 1%. The magnetic ordering associated with the lowest-energy converged solution is deemed to be that of the ground state. While the global UHF ground state in a disordered system, with many potential local energy minima, is in general unlikely to be thus found, we note the following: (i) Different AF startups (see Sec. II) typically converged to the same solution and invariably gave the lowest-energy final state, whatever its magnetic character. In

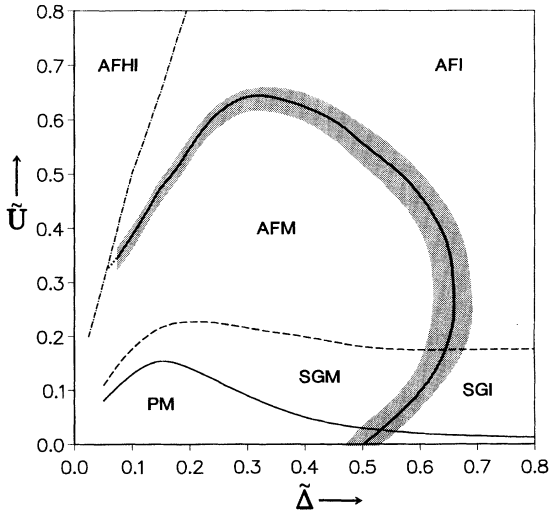

FIG. 2. Overall $y=1$ phase diagram. AF, antiferromagnet; SG, spin glass; P, paramagnet; M, metal; I, gapless insulator; HI, Hubbard insulator. The indicated region around the M-I boundary (thick, solid line) shows $0.05<\bar{L}(E_F)<0.07$.

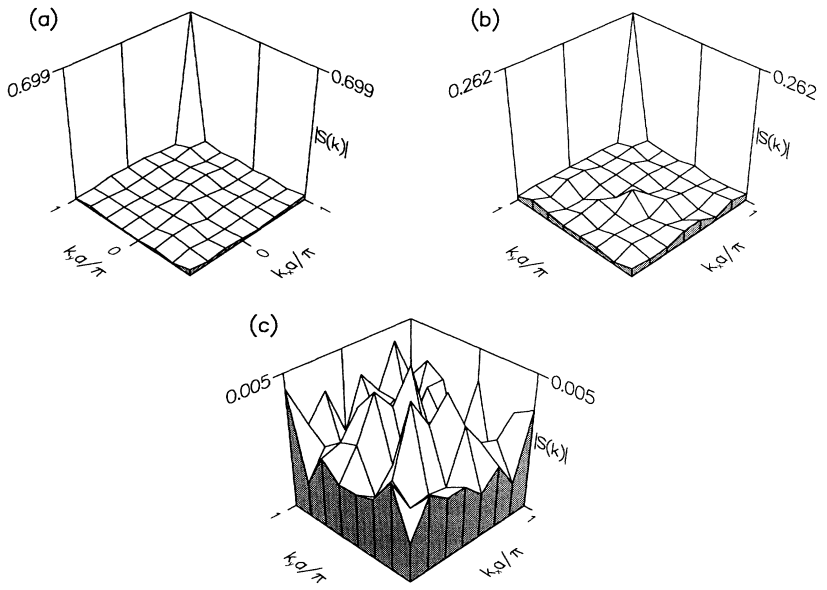

FIG. 3. Representative examples of $|S_z(\mathbf{k})|$ in the (k_x,k_y) plane with $k_z=\pi/a$. For $y=1$ with (a) $(\tilde{\Delta},\tilde{U})=(\frac{5}{12},1)$ (AF); (b) $(\tilde{\Delta},\tilde{U})=(\frac{5}{12},\frac{1}{2})$ (AF); and (c) $(\tilde{\Delta},\tilde{U})=(\frac{5}{12},0.15)$ (SG).

the AF region of Fig. 2 (and excepting the AF-SG border as explained below), the final state remained AF and lower-energy SG or P states were not found. (ii) Again excepting the AF-SG border, AF startups in the SG region evolved into SG final states; no AF converged solutions were obtained. (c) In the P region of Fig. 2, all startups converged to the same paramagnetic solution.

We are thus quite confident in our assignments for the magnetic character of the $y=1$ ground states. Further, the selected stability matrix and Heisenberg-spin UHF studies mentioned in Sec. II show that the lowest-energy solutions we obtain are indeed at least locally stable. One point should, however, be noted concerning the different converged UHF solutions accessed from different magnetic startups at a given $(\tilde{\Delta},\tilde{U})$ point. Namely the resultant distribution over lattice sites of local charges n_i and magnetic moment *magnitudes* $|\mu_i|$ are found to be almost identical for all such startups and are controlled primarily by the disorder realization of the bare site energies $\{\epsilon_i\}$. Differences between converged or final states thus stem largely from magnetic ordering—as dictated by the relative *phases* of the local moments $\{\mu_i\}$ [reflected in $S_z(\mathbf{k})$]—and not from significant variation, among the solutions, in the distribution of local moment magnitudes $\{|\mu_i|\}$.

The P-SG boundary in Fig. 2 is subject to uncertainty of approximately ± 0.02 in each of $\tilde{\Delta}$ and $\tilde{U}$, due largely to pointwise sampling of the phase plane, but appears to be robust: For a given $(\tilde{\Delta},\tilde{U})$ point in the P region, different disorder realizations yield almost exclusively P lowest-energy converged states, and similarly on the SG side of the boundary. While the data preclude a clear assessment of the order of the P-SG transition, the convergence characteristics of the iteration towards a final solution on either side of the P-SG border are suggestive of a first-order transition; and we note that for a half-filled nonbipartite fcc lattice the pure $(\tilde{\Delta}=0)$ Hubbard model at UHF level has a first-order transition from a paramagnetic to an ordered local moment phase (see, e.g., Ref. 32).

In contrast to the P-SG boundary, the SG-AF boundary is less well delineated, hence the dashed line in Fig. 2. This is particularly true for $\tilde{\Delta}\gtrsim 0.5$ where, for a given $(\tilde{\Delta},\tilde{U})$ point within approximately ± 0.05 of the boundary shown, an AF or SG lowest-energy final state may result according to the particular disorder realization, each occurring with significant measure.

To clarify this we note first that in the $\tilde{\Delta}=0$ nondisordered limit, the UHF ground state of the pure Hubbard model at half-filling is a two-sublattice *uniform* Néel antiferromagnet,[31] with local moments whose magnitudes $|\mu_0|$ are identical for all sites and thus coincide trivially with the mean local moment magnitude per site $|\mu|$ given generally by

$$|\mu| = N^{-1}\sum_i |\mu_i| \equiv \int_{-\infty}^{\infty} |\mu(\epsilon)| g(\epsilon) d\epsilon \ . \tag{3.1}$$

From (2.5) the corresponding $|S_z(\mathbf{k})|$ is thus nonzero only for $\mathbf{k}a/\pi=(1,1,1)$, with magnitude $|\mu_0|$. For a disordered AF, in contrast, there is typically considerable disorder in the distribution of local moment *magnitudes* $\{|\mu_i|\}$ over the sites as discussed below; but if the relative *phases* of the moments on sites with $|\mu_i|>0$ are appropriately "phaselocked," a disordered AF will result, again characterized by a strong peak in $|S_z(\mathbf{k})|$ at $\mathbf{k}a/\pi=(1,1,1)$, whose magnitude is on the order of the mean local moment magnitude per site $|\mu|$. This is seen in Fig. 3(a) for $(\tilde{\Delta},\tilde{U})=(\frac{5}{12},1)$: $|\mu|=0.71$, and the AF peak in $|S_z(\mathbf{k})|$ has magnitude 0.70.

The $|\mu|$ profile in the $(\tilde{\Delta},\tilde{U})$ plane is readily determined; here we simply note that $|\mu|\gtrsim 0.05$ for the AF region of the $y=1$ phase diagram, Fig. 2. As the interaction strength $\tilde{U}$ is progressively decreased towards the AF-SG border region from an AF regime, some phase mismatch of the local moments $\{\mu_i\}$ may occur, rendering the AF slightly "dirty." Nonetheless, the corresponding $|S_z(\mathbf{k})|$'s remain visibly dominated by the characteristic AF peak on the order of $|\mu|$, for the vast

majority of disorder realizations at a given $(\tilde{\Delta},\tilde{U})$ point [see, e.g., Fig. 3(b)]. Likewise, in approaching the SG-AF border region from the SG side, $|S_z(\mathbf{k})|$ for the lowest-energy states retains characteristic SG-like structure for almost all disorder realizations, with numerous randomly distributed small peaks in $S_z(\mathbf{k})$ and none dominant. In the AF-SG border region, however, we find the situation mentioned above of mixed AF or SG lowest-energy states according to the disorder realization at a given $(\tilde{\Delta},\tilde{U})$ point. A disorder average of $|S_z(\mathbf{k})|$ here would by itself suggest an AF phase, since the AF peaks in $|S_z(\mathbf{k})|$ will be reinforced on the average while the small random SG-like peaks will tend to wash out; but since SG lowest-energy states occur with significant measure, we do not regard $\langle |S_z(\mathbf{k})| \rangle$ as an appropriate diagnostic. Rather, the behavior mentioned hints at the absence of a direct AF-SG transition, with a possible two-phase region of not insignificant width; but further resolution is unfortunately difficult, since around the AF-SG border (where $|\mu| \simeq 0.05$) final-state energy differences are very small.

Although a magnetically ordered ground state results if the local moments are appropriately phase locked, it will nevertheless be significantly disordered due to the inhomogeneous distribution of local moment *magnitudes* over the sites. To examine this and relate it to the relative location of the different magnetic phases in the disorder-interaction plane, Fig. 4 shows disorder averages of the mean local moment magnitude per site of energy ϵ, $|\mu(\epsilon)|$ [Eq. (2.4)], and the corresponding mean local charge $n(\epsilon)$ for $(\tilde{\Delta},\tilde{U})=(\frac{5}{12},1)$ and $(\frac{5}{12},\frac{1}{2})$, where the system is a disordered AF [cf. Figs. 3(a) and 3(b)], and $(\tilde{\Delta},\tilde{U})=(\frac{5}{12},0.15)$ in a SG region [see Fig. 3(c)]; the corresponding atomic limit distributions described in Sec. II are also shown. For the AF examples, Figs. 4(a) and 4(b), the atomic limitlike character of the $|\mu(\epsilon)|/n(\epsilon)$ distributions is evident. The main effect of electron hopping processes (T) is to erode the distributions close to the local moment boundaries at $\tilde{\epsilon}=\epsilon/B \simeq \pm\frac{1}{2}\tilde{U}$. This narrows somewhat the $\tilde{\epsilon}$ range of sites with strong moments, and the extent of erosion increases with decreasing $\tilde{U}$ for fixed disorder $\tilde{\Delta}$. The essential characteristics of the atomic limit nonetheless remain evident for the $\tilde{U}=\frac{1}{2},1$ examples of Fig. 4: Strong atomiclike local moments persist on sites with bare site energies $\tilde{\epsilon}$ in a range of width $\sim\tilde{U}$ below the $y=1$ Fermi level at $\tilde{E}_F=E_F/B=\frac{1}{2}\tilde{U}$, the maximum such occurring at the center of the local moment range $\tilde{\epsilon}=0$ where $n(0)=1$.

In the AF regime—for both a given disorder realization, and over an ensemble of such—the ϵ dependence of the *mean* local moment magnitude per site of energy ϵ, $|\mu(\epsilon)|$, gives a good representation of the distribution of local moment magnitudes: Most sites in a narrow ϵ interval have moments close to the mean $|\mu(\epsilon)|$; while RMS fluctuations relative to the mean are most significant close to the $y=1$ local moment boundaries around $\tilde{\epsilon} \simeq \pm\frac{1}{2}\tilde{U}$, where $|\mu(\epsilon)|$ becomes small, they are not the dominant theme. This is not so for the small-$\tilde{U}$ SG phase (where the mean moment magnitude per site $|\mu| \lesssim 0.05$). The typical SG $|\mu(\epsilon)|$ of Fig. 4(c) shows very significant erosion of atomic limitlike behavior, with tiny $|\mu(\epsilon)|$'s in the range $|\tilde{\epsilon}| \lesssim \frac{1}{2}\tilde{U}$. In contrast to an AF phase, however, the SG phase is typified by significant local moment instabilities occurring on only a small fraction of sites with $|\tilde{\epsilon}| \lesssim \frac{1}{2}\tilde{U}$ for any given disorder realization. This arises

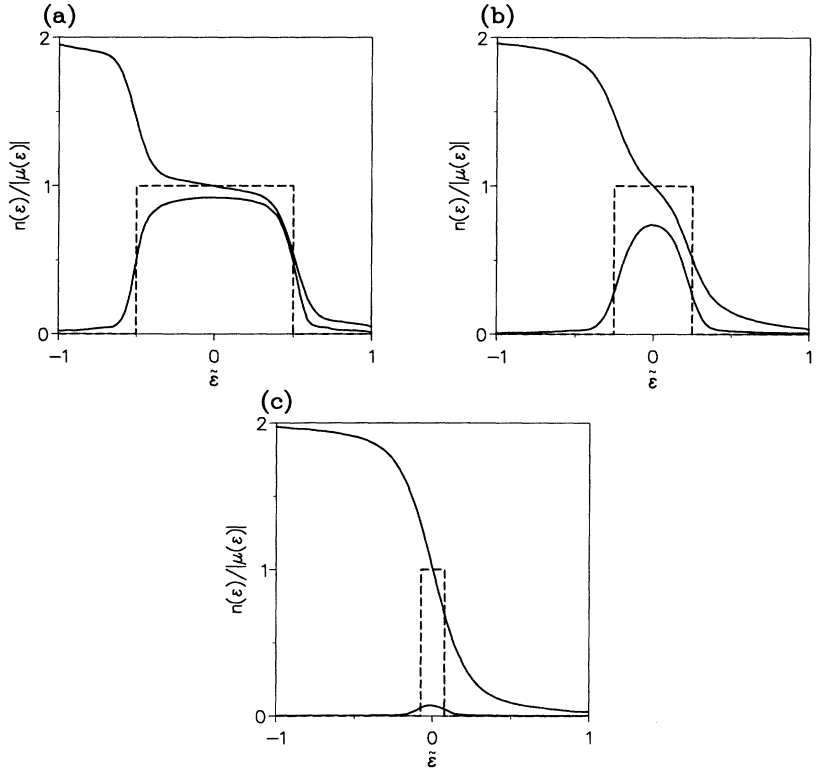

FIG. 4. $n(\epsilon)$ and $|\mu(\epsilon)|$ (solid lines) vs $\tilde{\epsilon}=\epsilon/B$, together with atomic limit $|\mu(\epsilon)|$ (dashed line) for $y=1$, $\tilde{\Delta}=\frac{5}{12}$, and (a) $\tilde{U}=1$, (b) $\frac{1}{2}$, and (c) 0.15.

from disorder-induced production of statistically rare local environments which favor the formation of strong atomiclike moments on only a small number of the sites with a given $|\tilde{\epsilon}| \lesssim \frac{1}{2}\tilde{U}$, the majority of such having very small (or no) moments.

The relative locations of the different magnetic phases in the $(\tilde{\Delta}, \tilde{U})$ plane (Fig. 2) may be rationalized from the above discussion. Dominance of the AF over the SG phase is naturally expected for larger $\tilde{U}$, where moments both become more stable and occur on a greater fraction of the sites. Similarly, one expects the SG phase to be favored over the nonmagnetic P phase for larger disorder $\tilde{\Delta}$ due to an enhanced probability of producing sites in rare local environments.

We comment finally on the nonmagnetic P phase in the $y=1$ site-disordered AHM. For *spatially* disordered AHM's, disorder in the distribution of hopping matrix elements $T_{ij}=T(|\mathbf{R}_i-\mathbf{R}_j|)$, arising from disorder in the site center-of-mass positions $\{\mathbf{R}_i\}$, also produces a range of local environments leading to local moment formation on an inhomogeneous scale.[18,22] Bhatt and Fisher[19] have recently argued against the occurrence of a P regime, and hence normal Fermi-liquid behavior, in such systems. They argue that at any mean site number density ρ_s, rare statistical density fluctuations will always lead to local moments on some sites; thus, even for low disorder (high ρ_s), some stable moments will persist. If applied to the present site-disordered AHM, these arguments might correspondingly suggest the absence of a P regime, the apparent presence of which in our calculations would thus be ascribed to finite-size effects. Two points should be noted in this regard: (i) In a recent finite-size numerical study at UHF level of a spatially disordered AHM with quenched liquidlike disorder,[22] we indeed appear to find what Bhatt and Fisher[19] suggest—significant moments on a few rare sites even at high mean densities and the absence of a true P regime. This is in contrast to the present work. (ii) The appearance of a P phase in the simple cubic site-disordered AHM would seemingly accord with the intuitive expectation that site disorder, in removing the characteristic Fermi surface nesting of the unperturbed $(U=0=\Delta)$ lattice, will lead to a P regime for sufficiently low $\tilde{U}$, analogous to the half-filled pure Hubbard model on nonbipartite cubic lattices. We believe it likely that this difference between the site-disordered and spatially disordered AHM is real. In the latter case, any site could potentially be in a rare region of low local density and thereby be able to sustain a moment. For the half-filled site-disordered model, in contrast, only sites within a relatively small $(\tilde{U} \lesssim \Delta \ll 1)$ width $\sim \pm\frac{1}{2}\tilde{U}$ of $\tilde{\epsilon}=0$ can potentially sustain local moments, as those with lower or higher $\tilde{\epsilon}$'s will be largely doubly occupied or empty, respectively; and sites with $\tilde{\epsilon} \simeq 0$ toward the center of $g(\epsilon)$ are those which are least likely to be surrounded by sites with widely differing $\tilde{\epsilon}$'s, and thus to have rare local environments.

IV. $y=1$ METALLIC AND INSULATING PHASES

For the half-filled noninteracting pure Anderson limit discussed in Sec. I, the system is metallic (insulating) for $\tilde{\Delta} < \tilde{\Delta}_c(1)$ $[\tilde{\Delta} > \tilde{\Delta}_c(1)]$ with $\tilde{\Delta}_c(1)=0.5$.[25–27] In the nondisordered pure Hubbard limit, in contrast, the half-filled bipartite system is a Mott-Hubbard insulator for all $\tilde{U}>0$, the Fermi level $E_F(1)=\frac{1}{2}U$ lying in a true Hubbard gap between the split lower and upper Hubbard bands in the pseudoparticle spectrum $D(E)$.[31] For the relatively weak-coupling interaction strengths considered here, however, the presence of only a small degree of site disorder is sufficient to broaden the Hubbard bands, eliminating the true gap and producing a pseudogap in $D(E)$, in which $E_F(1)$ lies. Insulating (I) or metallic (M) character is then determined by whether pseudoparticle states at E_F are localized or extended, assessed via the inverse participation ratio as described in Sec. II. We thus focus initially on the M-(gapless)I transition.

The Fermi level IPR profile $[\bar{L}(E_F)]$ in the $(\tilde{\Delta}, \tilde{U})$ plane for $y=1$ is shown in Fig. 5, obtained from $N=512$ site calculations. Projection of the appropriate threshold IPR, $\bar{L}_c=0.06$ [Eq. (2.9)] on to the $(\tilde{\Delta}, \tilde{U})$ plane gives the M-(gapless)I phase boundary shown in the full phase diagram, Fig. 2. The $\tilde{U}=0$ critical disorder, $\tilde{\Delta}_c(1)=0.5$ is correctly reproduced; the relative insensitivity of the location and features of the MI phase boundary to the chosen $\bar{L}_c$ is evident from the relative steepness of the $\bar{L}(E_F)$ profile around the $\bar{L}_c=0.06$ line on Fig. 5, and is also illustrated by the shaded region $0.05 < \bar{L}_c < 0.07$ shown in Fig. 2.

To illustrate the self-consistent pseudoparticle spectra and mean IPR $\bar{L}(E)$ as a function of energy E, Fig. 6 shows the disorder averaged total spectrum $D(E)$ at $y=1$ for fixed disorder $\tilde{\Delta}=\frac{5}{12}$ and for $\tilde{U}=0.5$ and 0.75; the corresponding $\bar{L}(E)$'s are also shown, together with mobility edges likewise inferred from $\bar{L}(E_c)=0.06$. With increasing $\tilde{U}$, $D(E_F)$ decreases and the pseudogap

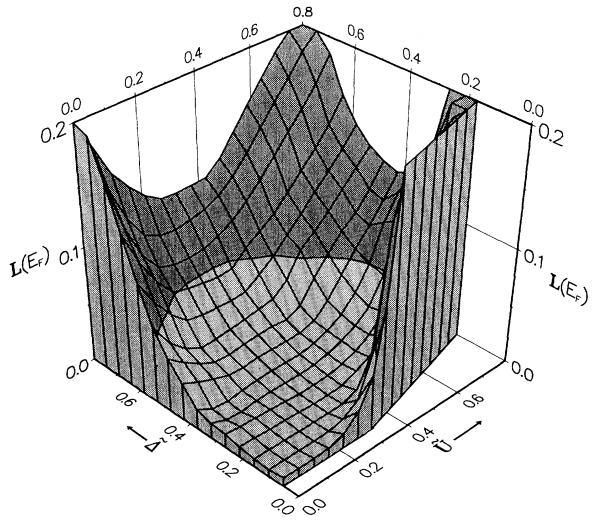

FIG. 5 Fermi-level IPR profile $\bar{L}(E_F)$ at half filling in the $(\tilde{\Delta}, \tilde{U})$ plane for $\tilde{\Delta}>0.05$ and $N=512$ site systems. The M-(gapless)I boundary obtained from $\bar{L}(E_F)=0.06$ is shown. The HI region (see text and Fig. 2) has been excised and the profile clipped at $\bar{L}(E_F)=0.2$.

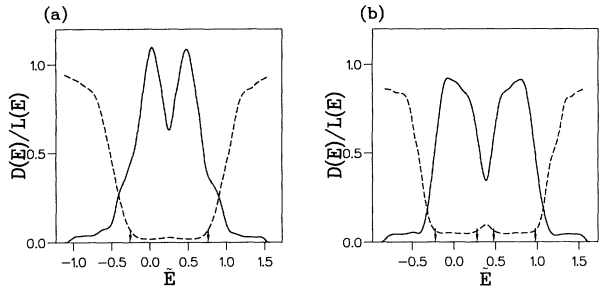

FIG. 6. Total spectrum $D(E)$ (solid line) vs $\tilde{E}=E/B$ at $y=1$ for $\tilde{\Delta}=\frac{5}{12}$ and (a) $\tilde{U}=0.5$ (AFM) and (b) $\tilde{U}=0.75$ (AFI). The dashed lines show $\bar{L}(E)$ for $N=512$, and the arrows show estimated mobility edges.

deepens; for $\tilde{U}=0.5$ states at $\tilde{E}_F=\frac{1}{2}\tilde{U}$ are delocalized and the system is an AFM, while for $\tilde{U}=0.75$ the system is an AFI. Although commensurate with the intuitive expectation that increasing $\tilde{U}$ in general enhances localization and hence the insulating phase, such behavior is not ubiquitous: For fixed $\tilde{\Delta}$ somewhat in excess of the $\tilde{U}=0$ critical disorder $\Delta_c(1)=0.5$, for example, Fig. 2 shows an interaction-induced I→M transition occurring at small interaction strengths, followed by the expected M→IT at larger $\tilde{U}$ values.[13,15]

To examine this microscopically we consider first the self-consistent distribution $f(\epsilon_{i\sigma})$ $[=f(\epsilon_{i-\sigma})]$ of effective σ-spin site energies $\epsilon_{i\sigma}=\epsilon_i+\frac{1}{2}U[n_i-\sigma\mu_i]$, which enter the UHF H_σ [Eq. (2.1)] and play essentially the same role in the disordered interacting system as the Gaussian distribution $g(\epsilon)$ of bare site energies does in the pure Anderson limit, and to which f trivially reduces for $\tilde{U}=0$. Figure 7 shows $f(\tilde{\epsilon}_{i\sigma})$ vs $\tilde{\epsilon}_{i\sigma}-\tilde{E}_F$ for fixed dis-

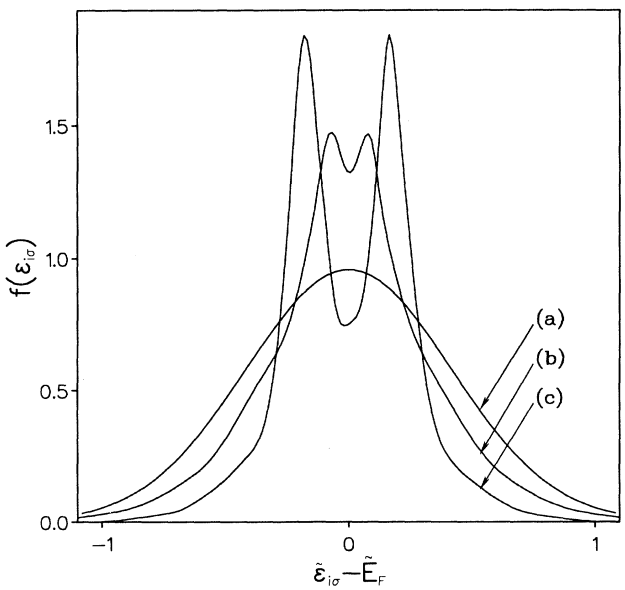

FIG. 7. The $y=1$ effective σ-spin site energy distribution $f(\epsilon_{i\sigma})$ vs $\tilde{\epsilon}_{i\sigma}-\tilde{E}_F$ for $\tilde{\Delta}=\frac{5}{12}$ and (a) $\tilde{U}=0$, (b) $\tilde{U}=\frac{1}{4}$, and (c) $\tilde{U}=\frac{1}{2}$.

order $\tilde{\Delta}=\frac{5}{12}$ and $\tilde{U}=$(a) 0, (b) 0.25, and (c) 0.5. For the smaller interaction strength $\tilde{U}=0.25$, the resultant $f(\tilde{\epsilon}_{i\sigma})$ is narrowed by an overall amount of order $\tilde{U}$ relative to the noninteracting $g(\epsilon)$. This arises because as noted by Ma[13] and Singh,[15] low-ϵ_i sites are significantly doubly occupied in the UHF ground state, with $\bar{n}_{i\sigma}\simeq 1\simeq\bar{n}_{i-\sigma}$ [see Fig. 9(b) below for $n(\epsilon)/|\mu(\epsilon)|$], so $\epsilon_{i\sigma}=\epsilon_i+U\bar{n}_{i-\sigma}$ exceeds ϵ_i by $\sim U$. The consequent narrowing of $f(\tilde{\epsilon}_{i\sigma})$ decreases the effective site disorder relative to $\tilde{U}=0$, increasing the fraction of sites with $\tilde{\epsilon}_{i\sigma}\simeq\tilde{E}_F$, which naturally participate most significantly in Fermi-level pseudoparticle states. This tends *per se* to stabilize the metallic phase for small $\tilde{U}$, as found by Ma[13] and Singh[15] in their macroscopic RG studies and is evidenced in the $y=1$ M-(gapless)I phase boundary of Fig. 2: For $0.5<\tilde{\Delta}\lesssim 0.65$ the system is insulating for $\tilde{U}=0$, but is initially driven metallic by increasing $\tilde{U}$. It is further seen in the Fermi-level IPR profile Fig. 5 where, for given $\tilde{\Delta}$, $\bar{L}(E_F)$ always decreases as the interaction strength is initially increased from zero. This holds even for $\tilde{\Delta}<0.5$ where the system is metallic for $\tilde{U}=0$, suggesting the likelihood of small-$\tilde{U}$ enhancement of the electrical conductivity in the metallic regime.

The first major effect of increasing $\tilde{U}$ from the noninteracting limit is to stabilize the metallic phase, as above. But as the interaction strength is increased further, and local moments increasingly stabilize on a progressively larger fraction of sites, a "pseudogap" develops in $f(\tilde{\epsilon}_{i\sigma})$, centered on $\tilde{\epsilon}_{i\sigma}=\tilde{E}_F$ $(=\frac{1}{2}\tilde{U})$, as illustrated in Fig. 7(c), by increasing $\tilde{U}$ to 0.5 for the chosen $\tilde{\Delta}=\frac{5}{12}$. A precursor of the pseudogap in $D(E)$, the pseudogap in $f(\tilde{\epsilon}_{i\sigma})$ deepens further with increasing $\tilde{U}$. Since the density of sites with $\tilde{\epsilon}_{i\sigma}\simeq\tilde{E}_F$—which thus participate most significantly in pseudoparticle states at $\tilde{E}_F$—drops significantly as $\tilde{U}$ is progressively increased, such sites are with increasing probability surrounded by sites with much higher or lower $\epsilon_{i\sigma}$'s such that the effective σ-spin site energy difference $|\Delta\epsilon_\sigma|$ is large compared to the hopping matrix element T, which connects them. Localization of pseudoparticle states thus ultimately occurs, and this is the dominant factor underlying the M→(gapless)IT occurring at $\tilde{U}\simeq 0.6$ for $\tilde{\Delta}=\frac{5}{12}$ as in Fig. 2. It is also seen in the $\bar{L}(E_F)$ profile of Fig. 5 where, for given $\tilde{\Delta}$, $\bar{L}(E_F)$ ultimately increases with increasing interaction strength.

Although the evolution of $f(\tilde{\epsilon}_{i\sigma})$ with $\tilde{U}$ gives useful insight into localization of pseudoparticle states, it does not by itself tell us *which* are the sites for which $\tilde{\epsilon}_{i\sigma}\simeq\tilde{E}_F$, and *why* their density decreases as $\tilde{U}$ is increased towards the M→I phase boundary. The answer to these questions provides a link between magnetism and the MIT, and is obtained by considering the Fermi-level charge density $H(\epsilon;E_F)$ defined in Sec. II.

For $(\tilde{\Delta},\tilde{U})=(\frac{5}{12},1)$ the system is an AFI at half-filling, with a reasonably deep pseudogap in $D(E)$ [Fig. 8(b)]. In Fig. 8(a), the disorder-averaged Fermi-level charge density is superimposed on the corresponding distribution of local charges $[n(\epsilon)]$ and magnetic moment magnitudes $[|\mu(\epsilon)|]$. This shows, as recently predicted,[21] that sites with strong atomiclike moments participate only weakly in *Fermi-level pseudoparticle states,* which are in contrast

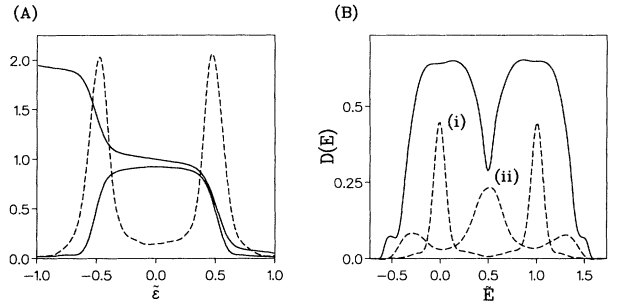

FIG. 8. (A) $n(\epsilon)/|\mu(\epsilon)|$ and $H(\epsilon;E_F)$ (dashed line) vs $\tilde{\epsilon}=\epsilon/B$ for $(\tilde{\Delta},\tilde{U})=(\frac{5}{12},1)$ and $y=1$. (B) Corresponding $D(E)$ vs $\tilde{E}$ (solid line); for (i) and (ii), see text.

dominated by sites with bare site energies $\tilde{\epsilon}$ close to the local moment boundaries, whose effective σ-spin site energies $\tilde{\epsilon}_{i\sigma}$ are close to the Fermi level $\tilde{E}_F(1)=\frac{1}{2}\tilde{U}$. As discussed in Ref. 21, the same correspondence holds also in the single-impurity Anderson model.[24]

The sites for which $\tilde{\epsilon}_{i\sigma}\simeq\tilde{E}_F$, which participate most significantly in Fermi-level states, are therefore those close to the local moment boundaries: the effective site energy for a σ-spin electron incident upon a site which is preferentially occupied by σ'-spin electrons (with $\sigma'=\pm\sigma$) is $\epsilon_{i\sigma}^{(\pm\sigma)}=\epsilon_i+\frac{1}{2}U[n_i\mp|\mu_i|]$, and sites with $\epsilon_i\simeq-\frac{1}{2}U$ close to the lower local moment boundary in $|\mu(\epsilon)|$ have $n_i+|\mu_i|\simeq 2$ [Fig. 8(a)], whence $\epsilon_{i\sigma}^{(-\sigma)}\simeq\frac{1}{2}U=E_F$. Conversely, sites close to the upper local moment boundary $\epsilon_i\simeq\frac{1}{2}U$ have $n_i-|\mu_i|\simeq 0$, whence $\epsilon_{i\sigma}^{(\sigma)}\simeq\frac{1}{2}U$ again. Why the density $f(\epsilon_{i\sigma})$ of sites with $\epsilon_{i\sigma}\simeq E_F$ decreases for given $\tilde{\Delta}$ as $\tilde{U}$ is increased towards the M$\rightarrow$I phase boundary [as in Fig. 7(c)] is also clear, for the fraction of sites with $\epsilon_i\simeq\pm\frac{1}{2}U$ close to the local moment boundaries decreases exponentially as $\sim\exp(-[\frac{1}{2}U]^2/2\Delta^2)$.

To support the above, Fig. 8(b) shows the $y=1$ disorder-averaged total pseudoparticle spectrum $D(E)$ vs $\tilde{E}$ for $(\tilde{\Delta},\tilde{U})=(\frac{5}{12},1)$. From (2.8) $D(E)$ may be deconvoluted in terms of the local spectra $D(\epsilon;E)$ appropriate to sites of energy ϵ. Figure 8(b) [curve (i)] shows the contribution from sites whose bare site energies lie within a small width $(\pm 0.075B)$ of $\epsilon=0$ where local moments $|\mu(\epsilon)|$ are a maximum [Fig. 8(a)]. This is essentially the local $D(\epsilon=0;E)$ and is seen to consist of well-resolved lower and upper Hubbard bands centered on $\tilde{E}\simeq 0$ and $\tilde{U}$, respectively, close to the corresponding effective σ-spin site energies $\tilde{\epsilon}_{i\sigma}^{(\sigma)}$ and $\tilde{\epsilon}_{i\sigma}^{(-\sigma)}$; such sites indeed give little contribution to states at $\tilde{E}_F=\frac{1}{2}\tilde{U}$ and are responsible for the twin peaks in $f(\epsilon_{i\sigma})$ evident in Fig. 7(c), whose separation is $\sim\tilde{\epsilon}_{i\sigma}^{(-\sigma)}-\tilde{\epsilon}_{i\sigma}^{(\sigma)}=\tilde{U}|\mu(0)|$. In contrast, curve (ii) of Fig. 8(b) shows the contribution to $D(E)$ from sites whose bare site energies are within a correspondingly small width of the local moment boundaries at $\tilde{\epsilon}\simeq\pm\frac{1}{2}\tilde{U}$. As expected from $H(\epsilon;E_F)$ vs $\tilde{\epsilon}$ [Fig. 8(a)], these contribute dominantly to states around $\tilde{E}\simeq\tilde{E}_F$ in the pseudogap, the absence of resolved Hubbard bands in the local spectrum reflecting the typically weak magnetic moments on such sites.

The above features persist as $\tilde{U}$ is decreased. $H(\epsilon;E_F)$ and the corresponding $n(\epsilon)/|\mu(\epsilon)|$ distributions are shown in Fig. 9 for $\tilde{\Delta}=\frac{5}{12}$ and $\tilde{U}=$ (a) 0.5, (b) 0.25, and (c) 0.025; for $\tilde{U}=0.5,0.25$ the system is an AF. Although $|\mu(\epsilon)|$ naturally erodes progressively as $\tilde{U}=U/12$ T decreases, significant moments persist for $|\tilde{\epsilon}|\lesssim\frac{1}{2}\tilde{U}$ and remain largest at $\tilde{\epsilon}=0$ where $n(0)=1$. In addition, as seen from $H(\epsilon;E_F)$, although reducing $\tilde{U}$ leads to states at E_F having increasing weight on sites with the strongest moments, they nonetheless remain dominated by sites close to the local moment boundaries. This is significant in particular for the $\tilde{U}=0.5$ example [Fig. 9(a)] where the system is an AF metal, in contrast to $\tilde{U}=1$, which is an AFI: There is still relatively *weak overlap of delocalized Fermi-level pseudoparticle states on strong local moment sites.* Thus, in the metallic phase, there is appreciable segregation of charge carriers and local moments, reminiscent of the assumptions which underly phenomenological two-fluid models (see, e.g. Refs. 9–11).

From Fig. 9, the fraction of moment carrying sites around $\tilde{\epsilon}\simeq 0$ decreases as $\tilde{U}$ is decreased further through the AFM and into the SGM phase, and the peaks in $H(\epsilon;E_F)$ merge to give a rather sharp distribution centered on $\tilde{\epsilon}=0$ which remains thus in the paramagnetic metallic regime as illustrated in Fig. 9(c). This implies that, at the P-SG boundary, where moments first stabilize on increasing $\tilde{U}$ from zero at given $\tilde{\Delta}$, the sites on which moments first stabilize will participate significantly in the delocalized Fermi-level states. This effect, which has been observed by Milovanović, Sachdev, and Bhatt[18] for a spatially disordered AHM, again provides a parallel to[18] the single-impurity Anderson model,[24] and is in agreement with the predictions of our recent statistical mean-field theory.[21]

The considerations above refer exclusively to gapless insulating and metallic phases at $y=1$. The final phase we consider is that of a Hubbard insulator (HI) where

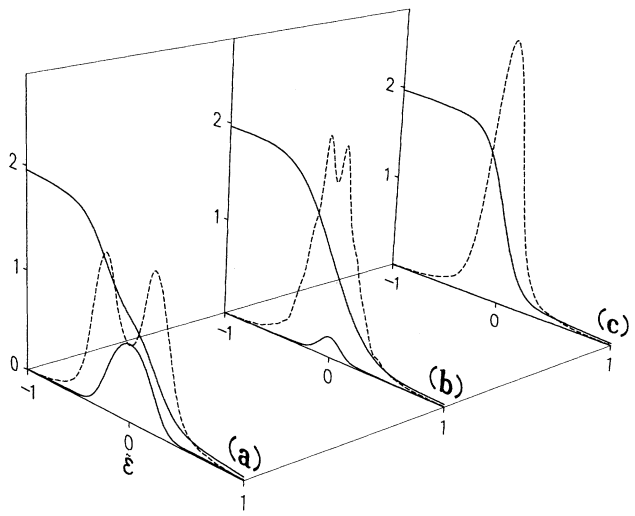

FIG. 9. $n(\epsilon)/|\mu(\epsilon)|$ and $H(\epsilon;E_F)$ (dashed line) vs $\tilde{\epsilon}$ at $y=1$ for $\tilde{\Delta}=\frac{5}{12}$ and (a) $\tilde{U}=\frac{1}{2}$, (b) $\tilde{U}=\frac{1}{4}$, and (c) $\tilde{U}=0.025$.

$E_F(1)$ lies in a true gap in the pseudoparticle spectrum $D(E)$. For the half-filled pure Hubbard-limit of no disorder, $\tilde{\Delta}=0$, such obtains for all $\tilde{U}>0$, the gap magnitude $\Phi_0(\tilde{U})$ increasing with $\tilde{U}$.[31] As $\tilde{\Delta}$ is increased from zero for given $\tilde{U}$, disorder will cause the Hubbard bands to overlap at some critical $\tilde{\Delta}_g(\tilde{U})$, eliminating the gap; since $\Phi_0(\tilde{U})$ increases with $\tilde{U}$ we expect $\tilde{\Delta}_g(\tilde{U})$ to increase with $\tilde{U}$. The HI phase is relevant to the MIT only if the transition is directly M→HI. This would imply the existence of a triple point $(\tilde{\Delta}_t,\tilde{U}_t)$ at which the M, gapless I, and HI phases coincide—where $\tilde{\Delta}_g(\tilde{U})$ intersects the M-(gapless)I phase boundary—and such that for $\tilde{\Delta}<\tilde{\Delta}_t$ the MIT with increasing $\tilde{U}$ is directly M→HI. Ma,[13] using a decimation renormalization-group approach, has estimated the triple point to be $(\tilde{\Delta}_t,\tilde{U}_t)\simeq(0.08,0.44)$.

As above, pseudoparticle states at $\tilde{E}_F(1)=\frac{1}{2}\tilde{U}$ in a pseudogap are dominated by sites with $|\tilde{\epsilon}|\simeq\frac{1}{2}\tilde{U}$ close to the local moment boundaries. For $\tilde{U}\gg\tilde{\Delta}$, the exponential tails in the site energy distribution $g(\tilde{\epsilon})$ clearly render difficult, in a finite-size calculation, an accurate determination of where a true gap opens; but our estimation of $\tilde{\Delta}_g(\tilde{U})$ is shown in the phase diagram of Fig. 2, and the following points should be noted: (a) The direct M-HI transition is clearly limited to a very small portion of the $(\tilde{\Delta},\tilde{U})$ plane, in a regime which is both weak coupling and weak disorder. For $\tilde{\Delta}\gtrsim 0.1$ we are fully confident that the MIT is M-(gapless)I, which is thus by far the dominant form of MIT in the phase plane. (b) Although we cannot strictly address the triple point, extrapolation of the $\tilde{\Delta}_g(\tilde{U})$ line and the M-(gapless)I boundary of Fig. 2 (dotted line) suggests $(\tilde{\Delta}_t,\tilde{U}_t)\simeq(0.06,0.33)$, agreeing adequately with Ma.[13] For $\tilde{\Delta}=0.05$ our numerical evidence is certainly consistent with a direct M→HI transition at a $\tilde{U}=\tilde{U}_c\simeq 0.3$: With $\tilde{U}$ just below $\tilde{U}_c$ the spectrum is clearly gapless, and incrementing $\tilde{U}$ by ~ 0.01 across $\tilde{U}_c$ produces a visible gap in $D(E)$ whose magnitude does not appear to be a statistical artifact and is largely insensitive to the disorder realization. (c) The seeming existence of a HI is consistent both with the ubiquity of such in the $\tilde{\Delta}=0$ limit and with the expectation that a small degree of disorder, in removing the strict Fermi-surface nesting of the simple cubic lattice, will produce the AFM→AFHI sequence with increasing $\tilde{U}$ that is characteristic of half-filled pure Hubbard models on nonbipartite cubic lattices.[32] Finally, although (see Sec. I) there is no gap in $D(E)$ for any U or $\Delta>0$ in the strict atomic limit $B=12T=0$, this limit corresponds to $\tilde{U}\to\infty$ and $\Delta\to\infty$ with $\tilde{U}/\tilde{\Delta}$ fixed and is thus far removed from the small $\tilde{\Delta}$ and $\tilde{U}$ domain relevant to the direct M→HI transition.

Finally, in relation to the $y=1$ magnetic phases of Sec. III, we note (a) that the small-$\tilde{U}$ paramagnetic phase is confined largely to the metallic regime as one might expect, since increasing disorder $\tilde{\Delta}$ favors both the I over the M phase and the SG over the P phase. (b) The small-$\tilde{U}$ interaction-induced I→MT occurs largely in the SG phase and the larger-$\tilde{U}$ "normal" M→IT in the AF phase, again as expected since increasing $\tilde{U}$ produces increasingly stable local moments on a progressively larger fraction of sites.

V. FILLING FRACTIONS $y<1$: MOTIVATION

In the pure $\tilde{\Delta}=0$ Hubbard limit for filling fractions $y<1$, the problem of magnetic ordering in the UHF ground state is formidable and has not to our knowledge been fully explored. Further, with $\tilde{\Delta}=0$, magnetic ordering may be intimately connected to electronic properties (see, e.g., Ref. 35), as also obtains at half filling for nonbipartite systems such as the triangular lattice, where a change in magnetic ordering at a critical U leads to the opening of a charge gap in $D(E)$ and hence an MIT.[30]

With disorder present to a non-negligible extent, however, and for the relatively small scaled interaction strengths $\tilde{U}$ examined here, we do not expect the essential neglect of magnetic ordering to be severe for the electronic characteristics we consider; for in the presence of disorder the electronic properties considered in the preceding sections—such as $D(E)$, $\bar{L}(E)$, and $H(\epsilon;E_F)$—appear quite insensitive to magnetic ordering. For example, very similar results are found if low-lying excited SG converged UHF solutions in the AF region of the $y=1$ phase diagram (Fig. 2) are considered. As discussed in Sec. III the distribution of local charges and moment *magnitudes* over the sites appear quite insensitive to magnetic ordering; as in Sec. IV, it is these that primarily control the properties of pseudoparticle states. To illustrate this, consider $(\tilde{\Delta},\tilde{U})=(\frac{5}{12},\frac{1}{2})$ where the correct $y=1$ ground state is AF. A typical $|S_z(\mathbf{k})|$ arising from a SG converged UHF solution at this point has the characteristic form of Fig. 3(c); but the corresponding $n(\epsilon)/|\mu(\epsilon)|$, $D(E)$, $\bar{L}(E)$, and $H(\epsilon;E_F)$ are barely distinguishable from those appropriate to the AF ground state [Figs. 4(b), 6(a), and 9(a)].

For $y<1$ we thus continue here with the Ising-spin UHF of Sec. II, and likewise with $S_z^{\rm tot}=0$ since, for the relatively small $\tilde{U}$'s examined, we do not consider the possibility of ferromagnetism. The phases of the local moments used for the initial or startup charge-moment distributions in the iterative self-consistent solution of the UHF equations will in general be taken here as randomly distributed over the sites, although we have considered a number of runs with magnetically ordered Ising startups, and with Heisenberg-spin UHF, to confirm that results are indeed not sensitive to the magnetic ordering in the converged UHF states.

For $y<1$, and largely for the reason of statistical control of low-ϵ sites, we also employ a cut Gaussian $g(\epsilon)$, nonzero in the interval $\epsilon_L=-\epsilon_U<\epsilon<\epsilon_U$. Provided $\epsilon_L\ll-\frac{1}{2}B$ the choice of cut is largely immaterial to us, and in practice we choose $\tilde{\epsilon}_L=\epsilon_L/B=-1$. We add that, for the scaled disorders $\tilde{\Delta}\lesssim 0.5$ considered here with $y<1$, the M-(gapless)IT phase boundary given in Fig. 2 at half filling for the pure Gaussian $g(\epsilon)$ is barely affected by the chosen cut. The main modification in introducing a cut in $g(\epsilon)$ naturally occurs at low filling fractions where, for sufficient low y in the strict atomic limit $B=12T=0$, all sites are either singly occupied or empty. This situation obtains up to $y=y'$ such that the atomic limit Fermi level $E_F(y')=\epsilon_L+U$; and $y'<1$ provided $U<2\epsilon_U$ (i.e., $\tilde{U}<2$ as considered here). For $y>y'$,

the atomic limit occupancy is as described in Sec. I for the pure Gaussian $g(\epsilon)$.

To motivate the $y<1$ work, we first consider the AHM at low filling fractions. The empty band limit $y=0$ is equivalent to the $\tilde{U}=0$ disordered tight-binding model (TBM), $D(E)$ for which at $\tilde{\Delta}=\frac{5}{12}$ is shown in Fig. 1(B) [for the pure Gaussian $g(\epsilon)$]. The AHM Hamiltonian (1.1) can be canonically transformed[36] from a site basis to a representation in terms of the exact eigenstates $\{|\Psi_\alpha^0\rangle\}$ of the noninteracting TBM, with basic operators, $c_{\alpha\sigma}^\dagger=\sum_i a_{i\alpha}c_{i\sigma}^\dagger$ and $c_{\alpha\sigma}$. Here $a_{i\alpha}$ is the coefficient of the site atomic orbital $|\phi_i\rangle$ in the expansion $|\Psi_\alpha^0\rangle=\sum_i a_{i\alpha}|\phi_i\rangle$ of the TBM eigenstate $|\Psi_\alpha^0\rangle$ of energy E_α, whose associated IPR is $L(E_\alpha)=\sum_i|a_{i\alpha}|^4$. This yields

$$H=\sum_{\alpha,\sigma}E_\alpha n_{\alpha\sigma}+\sum_{\alpha\beta\gamma\delta}U_{\alpha\beta\gamma\delta}c_{\alpha\uparrow}^\dagger c_{\beta\uparrow}c_{\gamma\downarrow}^\dagger c_{\delta\downarrow}\ , \tag{5.1}$$

with

$$U_{\alpha\beta\gamma\delta}=U\sum_i a_{i\alpha}^* a_{i\beta}a_{i\gamma}^* a_{i\delta}\ . \tag{5.2}$$

In the limit of no disorder where the $\{|\Psi_\alpha^0\rangle\}$ are extended Bloch states, and subject only to momentum conservation at the vertex, the interaction matrix elements $U_{\alpha\beta\gamma\delta}$ are state independent, reducing to $U_{\alpha\beta\gamma\delta}=U/N$. One does not therefore anticipate a tendency to interaction-induced local moment formation at sufficiently low y, commensurate with the intuitive expectation in nondisordered systems that interaction effects will be dominant at half-filling, diminishing in importance as the filling fraction y is reduced.

For disordered systems, in contrast, the interaction matrix elements $U_{\alpha\beta\gamma\delta}$ are strongly influenced by the localized or extended character of the $U=0$ TBM states. States in the lower region of the TBM spectrum—in particular those around and below the lower edge at $\tilde{E}=E/B=-\frac{1}{2}$ of the zero-disorder simple cubic spectrum—are naturally strongly localized due to the site disorder; see, e.g., Fig. 1(B). And at low filling fractions y, it is these localized, low-E TBM states which largely control the nature of the interacting system with $U>0$, since the more strongly localized the states are [i.e., the larger $\bar{L}(E)$], the greater the enhancement of electron interactions in suppressing double occupancy of the states, leading thereby to strong local moment formation. This is directly evident from (5.2) for the state diagonal element $U_\alpha=U_{\alpha\alpha\alpha\alpha}$, which reduces to $U_\alpha=UL(E_\alpha)$.

In fact, since the localization lengths ξ_α of low-energy TBM states decrease with increasing localization, we anticipate for sufficiently small filling fractions y an effective double exclusion principle whereby the ground state of the $U>0$ interacting system consists essentially of a narrow energy range of mainly nonoverlapping and singly occupied TBM states, and thus strong local moments associated with the occupied states which, although localized and nonoverlapping in space, are not atomically localized on single sites. Nevertheless, in such a y regime, we expect behavior strongly reminiscent of the true atomic limit of the model, since with $U_\alpha=U_{\alpha\alpha\alpha\alpha}$ dominant in (5.1) the AHM Hamiltonian reduces to

$$H\simeq\sum_{\alpha,\sigma}E_\alpha n_{\alpha\sigma}+\sum_\alpha U_\alpha n_{\alpha\uparrow}n_{\alpha\downarrow}\ , \tag{5.3}$$

which is formally similar to the true $B=12T=0$ limit of the AHM (1.1), but with $\epsilon_i\to E_\alpha$ and $U\to U_\alpha$. This simple Hamiltonian has been used successfully by Kamimura and Aoki (see, e.g., Refs. 4 and 36) in relation to the intermediate regime of doped, uncompensated semiconductors such as P:Si. For low electron filling fractions, y, qualitative considerations along the above lines have also been used by us[37] to rationalize the experimental behavior of binary monovalent alloys such as liquid $Cs_xAu_{1-x}\equiv Cs_y[CsAu]_{1-y}$, with electropositive Cs somewhat in excess of the stoichiometric composition ($x=\frac{1}{2},y=0$) where the system is a charge-transfer ionic insulator $\sim Cs^+Au^-$.

VI. $y<1$: RESULTS

We consider the evolution of the system with increasing filling fraction y up to the half-filled limit $y=1$. The variation of results with $\tilde{U}$ and $\tilde{\Delta}$ is considered in Sec. VI C. In Secs. VI A and VI B we focus first on fixed values of the scaled disorder and interaction strengths $(\tilde{\Delta},\tilde{U})=(\frac{5}{12},\frac{1}{2})$ where, as in Fig. 2, the system is a antiferromagnetic metal at $y=1$. For $\tilde{\Delta}=\frac{5}{12}$, we note that the fraction y_c of sites with bare site energies below the lower edge of the unperturbed simple cubic band (see Fig. 1) is $y_c\simeq 0.11$.

A. The quasiatomic regime

The qualitative arguments of Sec. V suggest, for sufficiently low filling fractions, the occurrence of a "quasiatomic" regime[21,37] where, as a consequence of the strong localization of states in the lower edge of the $\tilde{U}=0$ disordered TBM spectrum, the ground state of the $\tilde{U}>0$ interacting system consists essentially of a narrow energy range of predominantly nonoverlapping and singly occupied TBM states up to the Fermi level $E_F(y)$. In the limit of *strictly* nonoverlapping and singly occupied TBM states, the energy gain in removing an electron from an occupied TBM state of energy E_α is $E_\alpha<E_F(y)$, while the cost of adding an opposite spin electron to such is $E_\alpha+U_\alpha>E_F(y)$. Thus, as follows formally using (5.3), for $E<E_F(y)$ the spin-summed total density of single particle excitations (DOS) $D(E)$ reduces to $\frac{1}{2}D_0(E)$, with $D_0(E)$ the DOS for the $U=0$ noninteracting TBM limit. For E just in excess of $E_F(y)$, however, a single electron of either spin may be added to an unoccupied TBM state with energy cost E; hence as E crosses $E_F(y)$, the DOS jumps discontinuously to $D(E)=D_0(E)$.

In Fig. 10(A), for a filling fraction $y=0.05$, we show the disorder-averaged DOS $D(E)$ obtained from the self-consistent UHF calculations; occupied pseudoparticle states in $D(E)$ are shown shaded. The mean IPR $\bar{L}(E)$ for the pseudoparticle states is also included, confirming that occupied states are strongly localized and the system

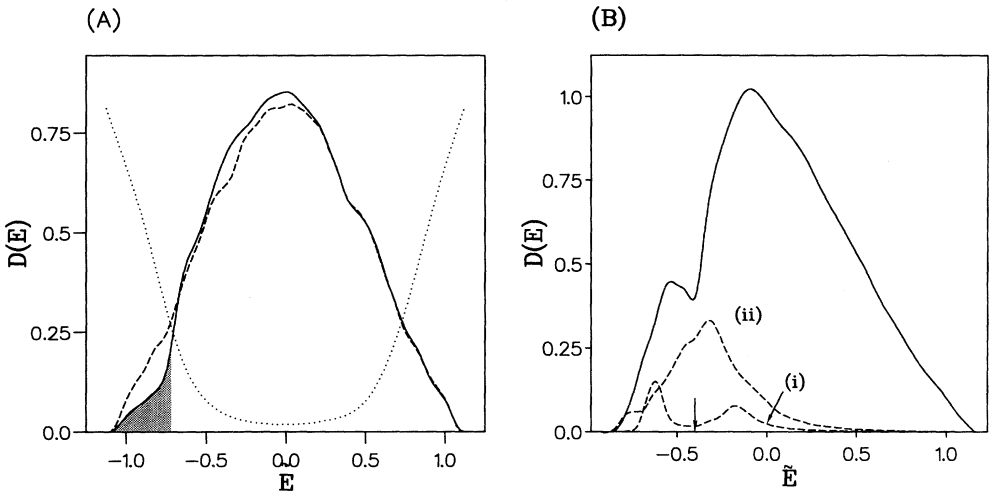

FIG. 10. Disorder-averaged spectrum $D(E)$ vs $\tilde{E}$ with $N=512$ sites for $(\tilde{\Delta},\tilde{U})=(\frac{5}{12},\frac{1}{2})$ and (A) $y=0.05$. Occupied pseudoparticle states are shaded. Also shown is $\bar{L}(E)$ for pseudoparticle states (dotted line) and the corresponding $\tilde{U}=0$ spectrum $D_0(E)$ (dashed line). (B) $y=0.25$. $E_F(y)$ is indicated by an arrow; for (i) and (ii) see text.

insulating. For comparison the corresponding noninteracting $D_0(E)$ is also shown, and the behavior mentioned above is indeed seen. [That the "step" at $D(E_F)$ is not strictly discontinuous is in part due to some slight overlap of occupied pseudoparticle states for $y=0.05$, but stems more significantly from statistical finite-size effects "blurring" the position of $E_F(y)$ for different disorder realizations.]

To show further the characteristics of the quasiatomic domain Fig. 11(a) gives, for $y=0.03$, disorder averages of the self-consistently determined $n(\epsilon)$ (dotted line) and $|\mu(\epsilon)|$ (solid line); $H(\epsilon;E_F)$ is also shown. From Fig. 11(a) it is seen that $n(\epsilon)\simeq|\mu(\epsilon)|$ for all ϵ. That is, for essentially all sites i, the site local charge $n_i=|\mu_i|$, the magnitude of the site local magnetic moment. The condition $n_i=|\mu_i|$ for all i is an obvious consequence of strictly

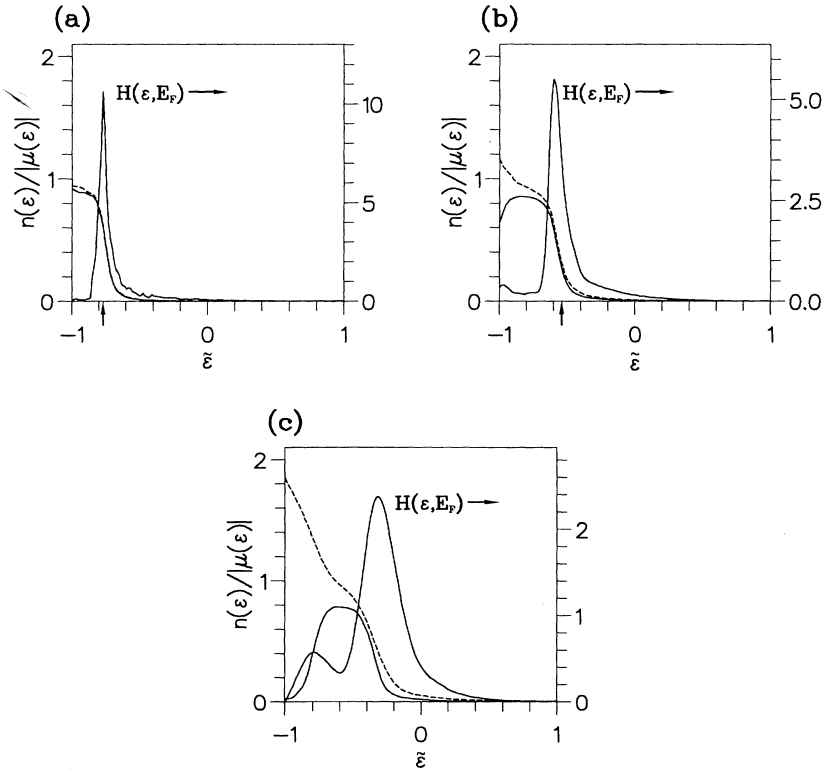

FIG. 11. (a) $n(\epsilon)$ (dashed line) and $|\mu(\epsilon)|$ (solid line) vs $\tilde{\epsilon}=\epsilon/B$ for $(\tilde{\Delta},\tilde{U})=(\frac{5}{12},\frac{1}{2})$ at $y=0.03$; the Fermi-level charge density $H(\epsilon;E_F)$ is also shown (right-hand scale), and the atomic limit Fermi level $\epsilon_F(y)$ is indicated by an arrow. (b) Same as (a), but for $y=0.095$. (c) Same as (a), but for $y=0.25$.

nonoverlapping singly occupied states for which all sites have zero double-occupancy probability, the quantum probability $P_{2i}=n_{i\uparrow}n_{i\downarrow}$ that site i is doubly occupied in the UHF ground state being $P_{2i}=\frac{1}{4}[n_i^2-\mu_i^2]$.

However, although occupied pseudoparticle states at low y are mainly singly occupied and nonoverlapping, they are not atomically localized on single sites but are, rather, typically spread over a small number of sites in the vicinity of one with a particularly low ϵ. This is reflected, for example, in the Fermi-level charge density $H(\epsilon;E_F)$ of Fig. 11(a). Although $H(\epsilon;E_F)$ is sharply distributed around $\epsilon=\epsilon_F(y)$ (the strict atomic limit Fermi level, shown by an arrow), indicating the dominant participation of such sites in Fermi-level pseudoparticle states, it has a nonzero width and a tail to higher $\epsilon>\epsilon_F(y)$ due to participation of these sites in states at E_F. As a corollary, sites with $\epsilon<\epsilon_F(y)$, which dominate pseudoparticle states of energy $E\simeq\epsilon$, have a nonvanishing probability of being unoccupied by electrons. This is reflected [Fig. 11(a)] in $n(\epsilon)<1$ for strongly occupied sites with $\epsilon<\epsilon_F(y)$: while $P_{2i}=0$ when $n_i=|\mu_i|$, the corresponding probabilities that site i is singly occupied or empty are given respectively by $P_{1i}=n_i$ and $P_{0i}=1-n_i$; only in the strict atomic limit, where $n_i=1$ $(=|\mu_i|)$ for all i with $\epsilon_i<\epsilon_F(y)$, is $P_{1i}=1$ and $P_{0i}=0$.

In the quasiatomic y regime the electrons are thus strongly localized and highly correlated. In qualitative terms this behavior persists up to a filling fraction of around $y_c\simeq 0.11$, the fraction of sites whose bare site energies lie below the lower edge of the simple cubic spectrum. This is evident from Fig. 11(b) for $y=0.095$, close to y_c.

B. Beyond the quasiatomic regime

For $y\gtrsim y_c$, a progressive deviation from quasiatomic behavior occurs. To illustrate this, Fig. 11(c) shows the self-consistently determined $n(\epsilon)/|\mu(\epsilon)|$ and $H(\epsilon;E_F)$ for $y=0.25$; corresponding results for half-filling, $y=1$, are given in Fig. 9(a). In the strict atomic limit, for filling fractions $y>y'$ $(\equiv y_c$ with $\tilde{U}=\frac{1}{2})$, sites with $\epsilon<\epsilon_F(y)-U$ are doubly occupied with $n(\epsilon)=1, |\mu(\epsilon)|=0$; the singly occupied local moment sites with $\epsilon_F-U<\epsilon<\epsilon_F(y)$ have $n(\epsilon)=1=|\mu(\epsilon)|$; and sites with $\epsilon>\epsilon_F$ have $n(\epsilon)=0=|\mu(\epsilon)|$. Strong double occupancy of low-ϵ sites is evident in Fig. 11(c), but although significant local moments persist on sites in an interval of width $\tilde{U}$ below $\epsilon_F(y)$, more significant erosion of atomic limit behavior is clearly occurring due to electron hopping effects reflected in $B=12T\neq 0$; even those sites with strong local moments have a not insignificant probability of being doubly occupied by electrons $[|\mu(\epsilon)|<n(\epsilon)]$.

In contrast to the $y=0.03$ example of Fig. 11(a), the Fermi-level charge density $H(\epsilon;E_F)$ for $y=0.25$ [whose vertical scale is markedly reduced from that of Fig. 11(a)] is more broadly distributed over a larger fraction of sites. As for the $y=1$ case [Fig. 9(a)], it is, however, evident that Fermi-level pseudoparticle states are again dominated by sites with bare site energies close to the local moment boundaries—the two peaks in $H(\epsilon;E_F)$ being separated by $\sim\tilde{U}$—and that the sites on which local magnetic moments are a maximum participate only rather weakly in states at E_F. This accords fully with the predictions of our statistical mean-field theory[21] and stems physically from the parallel between the site-disordered AHM and the single-impurity Anderson model[24] described in Ref. 21 (see also Sec. IV), whereby sites with bare site energies close to the local moment boundaries have effective σ-spin site energies which lie within a relatively small width of the Fermi level $E_F(y)$ to which states they thus dominantly contribute. We add further that, even for $y\neq 1$, the mean local charge $n(\epsilon_m)$ for sites with $\epsilon=\epsilon_m$ on which local moments are a maximum is indeed close to unity [Fig. 11(c)], again in agreement with the theory.[21]

To support the above remarks, the disorder-averaged total DOS $D(E)$ vs $\tilde{E}(=E/B)$ is shown in Fig. 10(b) for $y=0.25$, the Fermi level lying in the weak pseudogap evident in the spectrum. As in Eq. (2.8), $D(E)$ may be deconvoluted in terms of the local pseudoparticle spectra $D(\epsilon;E)$ pertaining to sites with given bare site energies ϵ. Curve (i) of Fig. 10(b) gives the contribution to $D(E)$ from sites with bare site energies lying within a small width $(\pm 0.075B)$ of $\epsilon=\epsilon_m$ where local moments $|\mu(\epsilon)|$ are a maximum [Fig. 11(c)]. From (2.8) this is essentially proportional to the local spectrum $D(\epsilon_m;E)$, which is thus seen to consist of clearly asymmetric, but well-resolved lower and upper Hubbard subbands. Commensurate with the $H(\epsilon;E_F)$ of Fig. 11(c), these strong local moment sites indeed give a very small contribution to the Fermi-level DOS $D(E_F)$, the Fermi level lying midway between the lower and upper Hubbard subbands in $D(\epsilon_m;E)$, in agreement with the theory of Ref. 21. Curve (ii) of Fig. 10(b) shows in contrast the contribution to $D(E)$ from sites whose bare site energies lie within a similarly small width of each of the two peaks in $H(\epsilon;E_F)$ [Fig. 11(c)], i.e., from sites close to the local moment boundaries in $|\mu(\epsilon)|$. As expected, and seen, these sites indeed give the dominant contribution to the pseudoparticle spectrum in the vicinity of the Fermi level E_F.

For both $y=0.25$, and at half filling $y=1$ where appreciable local moments persist for $(\tilde{\Delta},\tilde{U})=(\frac{5}{12},\frac{1}{2})$, the Fermi-level charge densities of Figs. 11(c) and 9(a) show that there is relatively weak overlap of pseudoparticle states at E_F on sites carrying strong local moments. With increasing filling fraction, however, it is clear that Fermi-level states are increasingly distributed over a larger fraction of sites. As suggested in Ref. 21, this may result in a transition from a gapless insulator (I) to a metal (M), with increasing filling fraction for given $(\tilde{\Delta},\tilde{U})$. That this is so in the present case is seen from Fig. 12(a) which, for $(\tilde{\Delta},\tilde{U})=(\frac{5}{12},\frac{1}{2})$ and $N=512$ site systems, shows the mean IPR $\bar{L}(E_F)$ for Fermi-level pseudoparticle states as a function of filling fraction y. For $y\lesssim y_c=0.11$ in the quasiatomic regime, pseudoparticle states at E_F are naturally strongly localized and the system insulating. This behavior clearly persists for y in excess of y_c; at $y=0.25$, for example, as in Fig. 10(b), the system remains a gapless insulator. With increasing y, however, $\bar{L}(E_F)$ steadily decreases. Adopting the thresh-

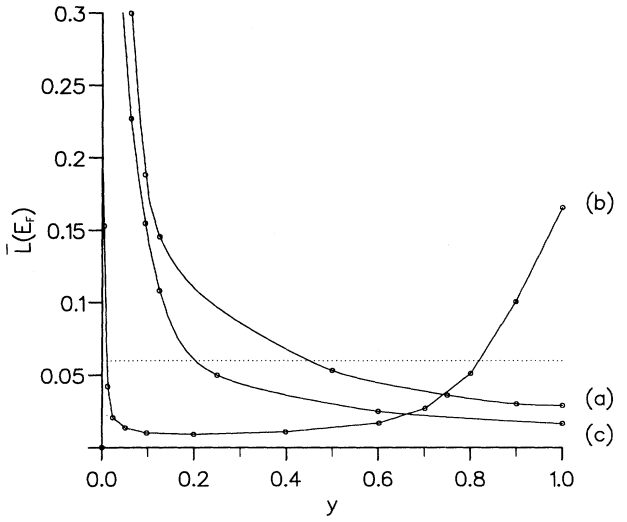

FIG. 12. The mean Fermi-level IPR $\bar{L}(E_F)$ as a function of filling fraction y, with $N=512$ site systems and for (a) $(\tilde{\Delta},\tilde{U})=(\frac{5}{12},\frac{1}{2})$; (b) (0.15,0.6); and (c) $(\frac{5}{12},\frac{1}{4})$. The dotted line shows $\bar{L}(E_F)=0.06\simeq\bar{L}_c(E_F)$.

old $\bar{L}_c(E_F)\simeq 0.06$ (as in Sec. II, although the qualitative results are evidently not sensitive to this choice), the system is already metallic by $y=\frac{1}{2}$, remaining so at half filling $y=1$.

Metallic behavior at half filling is not of course inevitable, as evident from the phase diagram Fig. 2. Provided appreciable moments persist we have seen above (see also Ref. 21) for any y that sites whose effective σ-spin site energies are close to the Fermi level, which thus give the dominant contribution to pseudoparticle states at $E_F(y)$, are those whose bare site energies are close to the local moment boundaries in $|\mu(\epsilon)|$, at $\epsilon\simeq E_F(y)$ and $E_F(y)-U$. At half-filling, $E_F(1)=\frac{1}{2}U$ by particle-hole symmetry; since the fraction of sites with $\epsilon\simeq\pm\frac{1}{2}U$ close to the local moment boundaries decreases exponentially as $\sim\exp(-[\frac{1}{2}\tilde{U}]^2/2\tilde{\Delta}^2)$, localization of Fermi-level states at $y=1$ is naturally expected as $\tilde{U}/\tilde{\Delta}$ is increased, as found in Sec. IV.

Figure 12 thus also shows the y dependence of $\bar{L}(E_F)$ for $(\tilde{\Delta},\tilde{U})=(0.15,0.6)$ curve (b), where at $y=1$ the system is a gapless insulator. As y is decreased from half filling, however, $E_F(y)$ progressively decreases from $\frac{1}{2}U$; and for a filling fraction y where $E_F(y)\simeq 0$, the probability density $g(\epsilon)$ of sites with $\epsilon\simeq E_F(y)\simeq 0$ which participate dominantly in pseudoparticle states at $E_F(y)$ is considerably enhanced. This leads one to expect the possibility of an insulator→metal transition with decreasing filling fraction from $y=1$, which is indeed evident in the figure: upon decreasing y an I→MT occurs at $y\simeq 0.82$. As y is decreased further, however, the system must ultimately revert again to an insulator due to the strong localization inexorable in the quasiatomic regime. This too is evident in Fig. 12(b) for $(\tilde{\Delta},\tilde{U})=(0.15,0.6)$, where the small-$y$ MIT naturally occurs at a much smaller filling fraction (since the reduction in $\tilde{\Delta}$ leads to a marked decrease in the fraction y_c of sites lying below the lower edge at $\tilde{E}=-\frac{1}{2}$ of the simple cubic spectrum).

C. Variation with $\tilde{U}$ and $\tilde{\Delta}$

We have so far considered the evolution with filling fraction for fixed values $(\tilde{\Delta},\tilde{U})=(\frac{5}{12},\frac{1}{2})$ of the scaled disorder and interaction strengths. While a (gapless) insulator→metal transition occurs with increasing y, reasonably strong local moments persist for all filling fractions with the chosen $(\tilde{\Delta},\tilde{U})$. At half filling $y=1$, as discussed in Secs. III and IV, a decrease in the interaction strength $\tilde{U}$ for given $\tilde{\Delta}$ leads to a reduction in local moment stability: a progressively smaller fraction of sites typically possesses steadily weakening moments.

To illustrate the differential effect of $\tilde{U}$ at different filling fractions, Fig. 13 shows the self-consistent $n(\epsilon)/|\mu(\epsilon)|$ for $(\tilde{\Delta},\tilde{U})=(\frac{5}{12},\frac{1}{4})$ at $y=0.01$ (a), 0.03 (b), 0.25 (c), and 1 (d); the corresponding $\bar{L}(E_F)$ vs y is shown in Fig. 12(c). Three points are evident. (i) For $y=0.01$, essentially strict quasiatomic limit behavior is seen, with $n_i=|\mu_i|$ for all sites. (ii) At $y=0.03$, some double occupancy of low-ϵ sites is beginning to occur, as expected from the true atomic limit for which the filling fraction y' at which double occupancy begins is $y\simeq 0.03$. This is analogous to $n(\epsilon)/|(\epsilon)|$ in Fig. 11(b) for $(\tilde{\Delta},\tilde{U})=(\frac{5}{12},\frac{1}{2})$ at $y=0.095$, atomic limit double occupancy in this case occurring at $y'=y_c=0.11$. (iii) Although local moments typically persist in an $\tilde{\epsilon}$ range of width $\tilde{U}=\frac{1}{4}$, there is clearly a much more rapid erosion of local moment stability with increasing filling fraction in comparison to the $(\tilde{\Delta},\tilde{U})=(\frac{5}{12},\frac{1}{2})$ results of Fig. 11, and only rather feeble moments persist at half filling.

To examine this further, we consider the mean magnitude of the site local magnetic moment *per electron* $|\mu_e|$ defined by

$$|\mu_e|=\left\langle N_e^{-1}\sum_i|\mu_i|\right\rangle ,$$

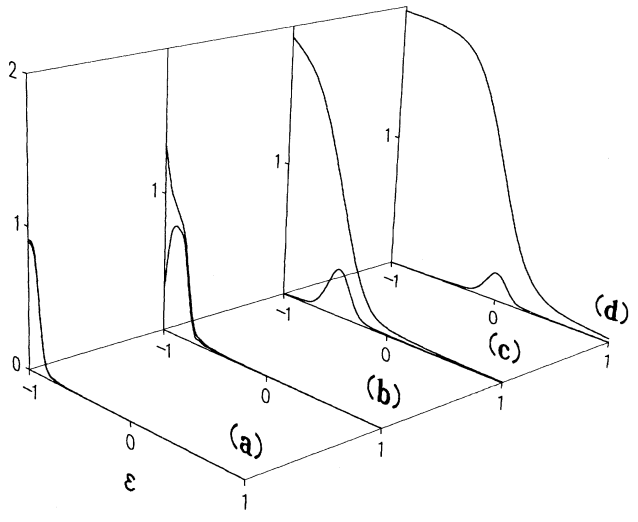

FIG. 13. $n(\epsilon)/|\mu(\epsilon)|$ vs $\tilde{\epsilon}=\epsilon/B$ for $(\tilde{\Delta},\tilde{U})=(\frac{5}{12},\frac{1}{4})$ and $y=0.01$ (a),0.03 (b), 0.25 (c), and $y=1$ (d).

with $N_e = yN$ the number of electrons. The y dependence of $|\mu_e|$ (with $N = 10^3$ site systems for $y \leq 0.25$) is shown in Fig. 14(A) for $(\tilde{\Delta}, \tilde{U}) = (\frac{5}{12}, \frac{1}{2})$ (i) and $(\frac{5}{12}, \frac{1}{4})$ (ii) where local moments exist at half filling. Also shown (iii) is $|\mu_e|$ for $(\tilde{\Delta}, \tilde{U}) = (0.15, 0.10)$. At half filling in this case the system cannot support local moments and is a paramagnetic metal (see Fig. 2); as seen from (iii) the same situation occurs for $y = 0.75$, while very weak moments are evident for $y = \frac{1}{2}$.

Regardless of whether local moments persist around half filling, however, it is clear in all cases that the characteristics of the quasiatomic regime are recovered at low filling fractions,[21] for as y is decreased and E_F moves progressively towards the edge of $D(E)$, occupied pseudoparticle states are increasingly dominated by low-ϵ sites, and their localization will ultimately produce strong enhancement of interaction effects and hence strong local moments. In fact, since $\langle N_e^{-1} \sum_i n_i \rangle = 1$ by charge conservation, it follows that $|\mu_e| = 1$ for a strict quasiatomic limit of totally nonoverlapping singly occupied states ($n_i = |\mu_i|$), reflecting the effective double exclusion principle for the occupied pseudoparticle states. In consequence, at a given filling fraction y where such obtains, a further increase in the interaction strength $\tilde{U}$ will obviously not change the occupancy of the states. This is evident in (i) and (ii) of Fig. 14(A) with $\tilde{\Delta} = \frac{5}{12}$, where at a filling fraction $y = 0.01$, $|\mu_e| \simeq 1$ is unaltered when $\tilde{U}$ is increased from $\frac{1}{4}$ to $\frac{1}{2}$.

For the $(\tilde{\Delta}, \tilde{U})$'s shown in Fig. 14(A), local moments become increasingly stable as y is decreased from half filling. For nondisordered systems, in contrast, the reverse trend is more typically expected, with half-filling being optimal for local moment formation. To illustrate the relative effects of disorder, Fig. 14(B) shows $|\mu_e|$ vs y for a fixed interaction strength $\tilde{U} = \frac{1}{2}$ and progressively decreasing scaled disorders, $\tilde{\Delta} = \frac{5}{12}$ (i), 0.15 (ii), and 0.05 (iii), where at half filling (see Fig. 2) the system is, respectively, an antiferromagnetic metal, gapless insulator, and Hubbard insulator. In agreement with Ref. 21, it is seen from Fig. 14(B) that at half filling local moments become increasingly stable as the disorder $\tilde{\Delta}$ is decreased while at lower filling fractions this trend is reversed. In particular, it is clear that upon decreasing $\tilde{\Delta}$ half filling indeed becomes optimal for local moment formation in the sense that $|\mu_e|$ decreases significantly as y is initially reduced from the half-filled limit. However, although $|\mu_e|$ is shown only down to $y = 0.01$, it is equally clear even for the weak-disorder cases that the quasiatomic regime again naturally emerges at sufficiently small filling fractions, as reflected in the small-y upturn in $|\mu_e|$.

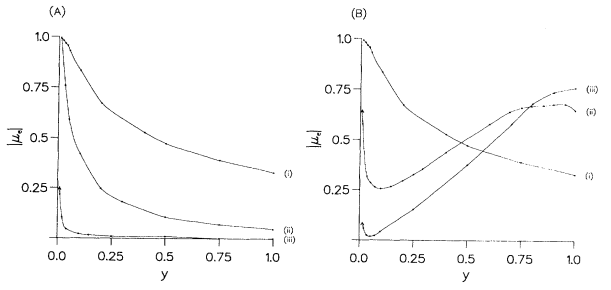

FIG. 14. The mean local moment magnitude per electron $|\mu_e|$ vs y for (A) $(\tilde{\Delta}, \tilde{U}) = (\frac{5}{12}, \frac{1}{2})$ (i), $(\frac{5}{12}, \frac{1}{4})$ (ii), and (0.15,0.1) (iii), and (B) for $\tilde{U} = \frac{1}{2}$ and $\tilde{\Delta} = \frac{5}{12}$ (i), 0.15 (ii), and 0.05 (iii).

VII. CONCLUSION

We have assessed numerically the UHF phase diagram (Fig. 2) for a Gaussian site-disordered Anderson-Hubbard model on a simple cubic lattice and at half filling $y = 1$. Magnetic phases (AF, SG, and P) and electric phases (M, gapless-I, HI) were each considered and characterized, and all relevant phase boundaries are found to occur in a relatively weak-coupling regime. The evolution with filling fraction y has also been considered for representative $(\tilde{\Delta}, \tilde{U})$ points. The disorder-induced enhancement of electron interactions in leading to local moment formation is found to be differential in y, leading in particular to a low-y "quasiatomic" regime of strong local moments and mainly singly occupied nonoverlapping pseudoparticle states, regardless of the existence of moments around half-filling.

We have sought in particular to give a microscopic explanation for observed behavior, central to which is the inhomogeneous distribution of charge and magnetization over the sites, reflected in the site energy dependence of $n(\epsilon)/|\mu(\epsilon)|$. Broadly speaking, the interaction strength U determined the ϵ range of sites which typically sustain local moments; U/Δ determines the fraction of moment carrying sites; and for given U, Δ the hopping matrix elements embodied in the unperturbed simple cubic bandwidth $B = 12$ T determine the extent of ϵ-differential local moment erosion, which is most pronounced towards the local moment boundaries and least significant for sites on which local moments, when they occur, are strongest. These factors enable us, for example, to rationalize the relative location in the $(\tilde{\Delta}, \tilde{U})$ phase plane of the $y = 1$ magnetic phases; see Sec. III.

A central link between magnetism and electronic properties stems from the fact that the sites which participate most significantly in Fermi-level pseudoparticle states are those with bare site energies close to the local moment boundaries in $|\mu(\epsilon)|$, in parallel to the single-impurity Anderson model[24] and in agreement with recent predictions.[21] In consequence, a combination of the Fermi-level charge density $H(\epsilon; E_F)$ and the probability density $f(\epsilon_{i\sigma})$ of effective σ-spin site energies, when used in conjunction with the Fermi-level IPR, $\bar{L}(E_F)$, enables a rationalization of the MIT and corresponding MI phase boundaries, in terms of an interplay between disorder and electron interactions. Conversely, it is found that as local moments increasingly stabilize on a larger fraction of sites, those on which moments are strongest participate increasingly weakly in pseudoparticle states at E_F. One upshot of this, for example, is that in a metallic regime with local moments, there is relatively weak overlap of delocalized Fermi-level pseudoparticle states on sites with strong local moments, i.e., appreciable segregation of charge carriers and local moments.

Finally we add that while UHF is mean field in the in-

teraction strength for any disorder realization, it permits a broad microscopic picture of the interplay between disorder and electron interactions. The resultant range of physical behavior in a weak-coupling regime is quite rich, even at this single-particle level, and we believe a sound understanding of such to be an important prerequisite to the systematic inclusion of many-body effects, particularly in the *disordered* interacting system; work in this direction is currently in progress.

ACKNOWLEDGMENTS

Helpful discussions with J. Cullum, C. Dasgupta, P. P. Edwards, D. S. Fisher, T. Koslowski, H. R. Krishnamurthy, P. A. Madden, W. von Niessen, H. Reinholz, F. Siringo, Y. H. Szczech, M. D. Winn, and P. Wölfle are gratefully acknowledged. C. Dasgupta is thanked for supplying a copy of Ref. 20. M.A.T. acknowledges the financial support of the SERC.

[1]N. F. Mott, *Metal-Insulator Transitions* (Taylor & Francis, London, 1974).
[2]P. A. Lee and T. V. Ramakrishnan, Rev. Mod. Phys. **57**, 287 (1985).
[3]E. L. Efros and M. Pollack, *Electron-Electron Interactions in Disordered Systems* (North-Holland, Amsterdam, 1985).
[4]H. Kamimura and H. Aoki, *The Physics of Interacting Electrons in Disordered Systems* (Clarendon, Oxford, 1989).
[5]E. Abrahams, P. W. Anderson, P. A. Lee, and T. V. Ramakrishnan, Phys. Rev. B **24**, 6783 (1981).
[6]A. M. Finkelstein, Zh. Eksp. Teor. Fiz. **84**, 168 (1983) [Sov. Phys. JETP **57**, 97 (1983)].
[7]C. Castellani, C. DiCastro, P. A. Lee, and M. Ma, Phys. Rev. B **30**, 527 (1984).
[8]C. Castellani, B. G. Kotliar, and P. A. Lee, Phys. Rev. Lett. **56**, 1179 (1986).
[9]Z. Z. Gan and P. A. Lee, Phys. Rev. B **33**, 3595 (1986).
[10]S. Sachdev, R. N. Bhatt, and M. A. Paalanen, J. Appl. Phys. **63**, 4285 (1988).
[11]S. Sachdev, Phys. Rev. B **39**, 5297 (1989).
[12]D. Belitz and T. Kirkpatrick, Phys. Rev. Lett. **63**, 1296 (1989).
[13]M. Ma, Phys. Rev. B **26**, 5097 (1982).
[14]A. Shimizu, H. Aoki, and H. Kamimura, J. Phys. C **19**, 725 (1986).
[15]A. Singh, Phys. Rev. B **37**, 430 (1988).
[16]G. T. Zimanyi and E. Abrahams, Phys. Rev. Lett. **64**, 2719 (1990).
[17]D. E. Logan and M. A. Tusch, J. Non-Cryst. Solids **156-158**, 639 (1993).
[18]M. Milovanović, S. Sachdev, and R. N. Bhatt, Phys. Rev. Lett. **63**, 82 (1989).
[19]R. N. Bhatt and D. S. Fisher, Phys. Rev. Lett. **68**, 3072 (1992).
[20]C. Dasgupta and J. W. Halley, Phys. Rev. B **47**, 1126 (1993).
[21]D. E. Logan and F. Siringo, J. Phys.: Condens. Matter **5**, 1841 (1993).
[22]D. E. Logan, I. J. Bush, and P. A. Madden, Z. Phys. Chem. (to be published).
[23](a) J. R. Schrieffer, Z.-G. Wen, and S.-C. Zhang, Phys. Rev. B **39**, 11 663 (1989); (b) A. Singh and Z. Tesanović, *ibid.* **41**, 614 (1990).
[24]P. W. Anderson, Phys. Rev. **124**, 41 (1961).
[25]C. M. Soukoulis, A. D. Zdetsis, and E. N. Economou, Phys. Rev. B **34**, 2253 (1986).
[26]B. Bulka, M.Schreiber, and B. Kramer, Z. Phys. B **66**, 21 (1987).
[27]T. M. Chang, J. D. Bauer, and J. L. Skinner, J. Chem. Phys. **93**, 8973 (1990).
[28]M. W. Long, in *The Hubbard Model; Recent Results,* edited by M. Rasetti (World Scientific, London, 1991).
[29]J. E. Hirsch, Phys. Rev. B **22**, 5259 (1980); **31**, 4403 (1985).
[30]C. Jayaprakash, H. R. Krishnamurthy, S. Sarker, and W. Wenzel, Eurosphys. Lett. **15**, 625 (1991).
[31]D. R. Penn, Phys. Rev. **142**, 350 (1966).
[32]D. Grensing, E. Marsch, and W.-H. Steeb, Phys. Rev. B **17**, 2221 (1978).
[33]D. J. Thouless, *The Quantum Mechanics of Many-Body Systems* (Academic, New York, 1972).
[34]J. Cullum and R. A. Willoughby, *Lanczos Algorithms for Large Symmetric Eigenvalue Computations, Progress in Scientific Computing Series* (Birkhäuser, Boston, 1984), Vols. 1 and 2.
[(35)]H. J. Schulz, Phys. Rev. Lett. **64**, 1445 (1990).
[36]H. Kamimura, Philos. Mag. B **42**, 763 (1980).
[37]D. E. Logan and F. Siringo, J. Phys. Condens. Matter **4**, 3695 (1992).